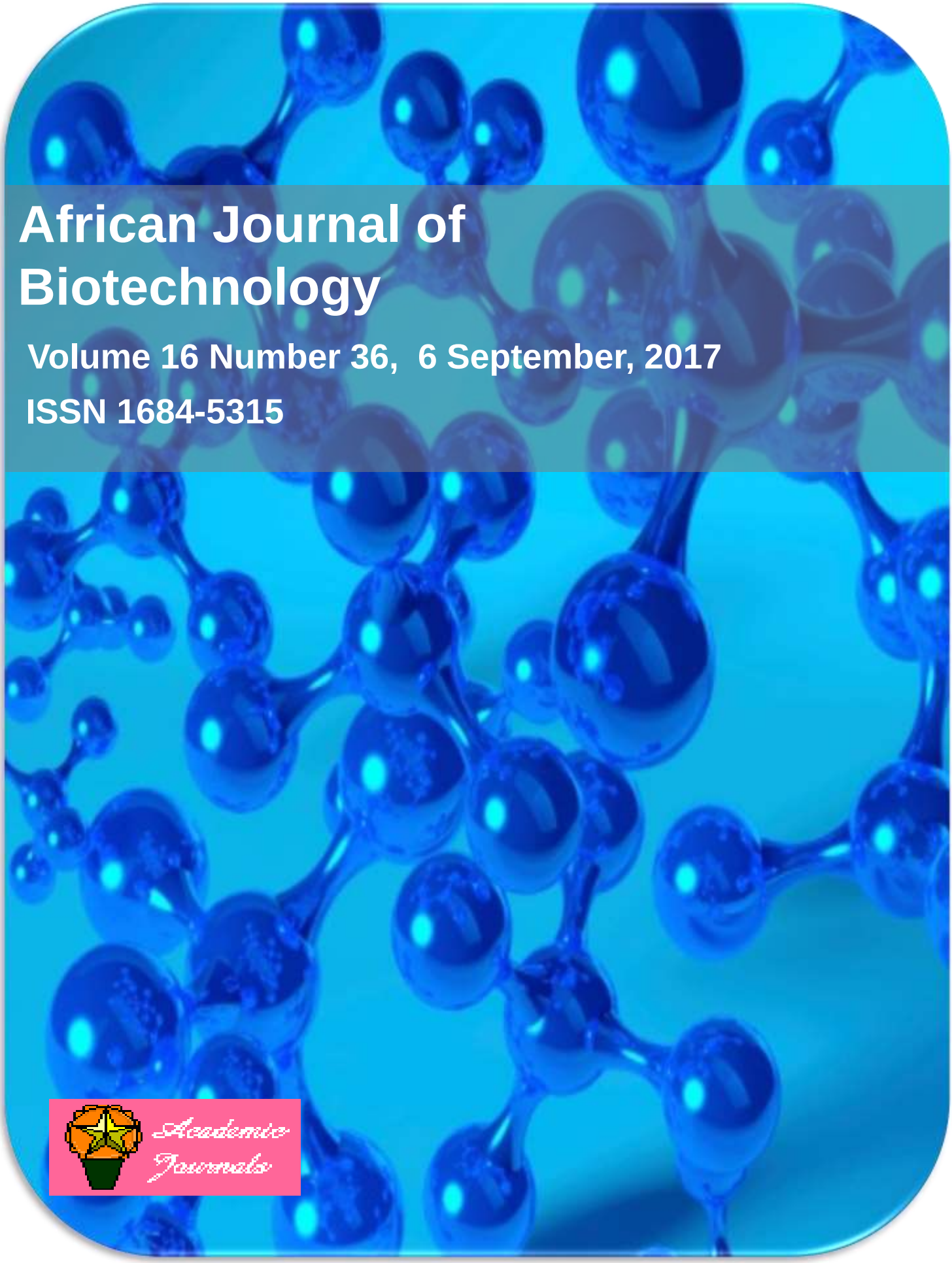

African Journal of Biotechnology

Volume 16 Number 36, 6 September, 2017
ISSN 1684-5315

Academic Journals

ABOUT AJB

The African Journal of Biotechnology (AJB) (ISSN 1684-5315) is published weekly (one volume per year) by Academic Journals.

African Journal of Biotechnology (AJB), a new broad-based journal, is an open access journal that was founded on two key tenets: To publish the most exciting research in all areas of applied biochemistry, industrial microbiology, molecular biology, genomics and proteomics, food and agricultural technologies, and metabolic engineering. Secondly, to provide the most rapid turn-around time possible for reviewing and publishing, and to disseminate the articles freely for teaching and reference purposes. All articles published in AJB are peer-reviewed.

Contact Us

Editorial Office: ajb@academicjournals.org

Help Desk: helpdesk@academicjournals.org

Website: http://www.academicjournals.org/journal/AJB

Submit manuscript online http://ms.academicjournals.me/

Editorial Board

African Journal of Biotechnology

Table of Content: Volume 16 Number 35 6 September, 2017

ARTICLES

academicJournals

Vol. 16(36), pp. 1819-1825, 6 September, 2017
DOI: 10.5897/AJB2017.15967
Article Number: 8E8B2BA65873
ISSN 1684-5315

http://www.academicjournals.org/AJB

African Journal of Biotechnology

Full Length Research Paper

Production, optimization and characterization of silver oxide nanoparticles using *Artocarpus heterophyllus* rind extract and their antifungal activity

Velu Manikandan[1], Pyong-In Yi[2], Palanivel Velmurugan[1], Palaniyappan Jayanthi[3], Sung-Chul Hong[2], Seong-Ho Jang[2], Jeong-Min Suh[2] and Subpiramaniyam Sivakumar[2]*

[1]Division of Biotechnology, Advanced Institute of Environment and Bioscience, College of Environmental and Bioresource Sciences, Chonbuk National University, Iksan, Jeonbuk 54596, South Korea.
[2]Department of Bioenvironmental Energy, College of Natural Resource and Life Science, Pusan National University, Miryang-si, Gyeongsangnam-do, 627-706, Republic of Korea.
[3]Department of Environmental Science, Periyar University, Salem, 636011, Tamil Nadu, India.

Received 1 March, 2017; Accepted 16 May, 2017

For the first time, the phytochemical fabrication of noble silver oxide nanoparticles was reported using *Artocarpus heterophyllus* rind extract as well as their characterization. The UV-vis absorption spectrum of the phytochemical-mediated reduced reaction mixture showed a surface plasmon peak at 428 nm, which confirmed the presence of silver nanoparticles. The silver nanoparticle production was ideal at pH 9 with 2.0 mL jackfruit rind extract, Ag^+ 1.0 mM and 180 min of reaction time. Fourier transform infrared spectroscopy analysis indicated the presence of acids, esters, alcohols, pyrazine, etc. which can act as capping agents around the nanoparticles. X-ray diffraction analysis confirmed the face-centered cubic crystalline and the oxygen structure of metallic silver nanoparticles. The average diameter of silver nanoparticles is ~17 nm via high resolution transmission electron microscopy, which agrees with the average crystallite size (24.2 nm) calculated from X-ray diffraction analysis and selected area electron diffraction pattern. Of the five tested phytopathogens, the pathogens *Phytophthora capsici, Colletotrichum acutatum* and *Cladosporium fulvum* showed 8, 11 and 16 mm zones of inhibition against synthesized silver oxide nanoparticles at 200 µg/well, respectively.

Key words: Silver oxide, nanoparticle, antifungal, plant pathogen, optimization.

INTRODUCTION

Metallic silver has gained much attention for its greener and faster synthesis approaches as well as biomedical, industrial and pharmaceutical applications. It has important chemical, thermal and photo catalytic properties. Physical and chemical methods have been employed to synthesize metal nanoparticles, but these

*Corresponding author. E-mail: ssivaphd@yahoo.com. Tel: +82-55-350-5431. Fax: +82-55-350-5439.

Figure 1. Jackfruit whole tree, rind, rind powder, and the presence of silver nanoparticle confirmation by color change in the reaction mixture.

are hazardous, toxic and expensive (Velmurugan et al., 2016). Hence, the scientific community has turned their attention towards low cost and eco-friendly synthesis of silver nanoparticles from biological sources like plants and microbes (Lee et al., 2016). The bio- and phyto-synthesized silver nanoparticles are non-toxic, ecofriendly and viable. Leaves, fruits, stems, roots, bark and latex have all been used to prepare metallic nanoparticles (Nazeruddin et al., 2014).

Silver nanoparticles with unique physical, chemical and biological properties are certainly the most extensively used nanoparticles in wound dressings, antimicrobial coatings, anti-cancer chemotherapy and cosmetics (Kim et al., 2012). Silver exhibits multiple modes of inhibitory action against microorganisms, which has been used for several years. Silver nanoparticles are common antimicrobial agents because their production costs are low (Lamsal et al., 2011).

According to literature, silver nanoparticles were synthesized from *Tribulus terrestris* (Mariselvam et al., 2014), *Pistacia atlantica* (Sadeghi et al., 2015), *Calotropis procera* (Gondwal and Pant, 2013), *Musa paradisiacal* (Bankar et al., 2010), *Citrus sinensi* (Kaviya et al., 2011), *Eucalyptus hybrid* (Dubey et al., 2009), *Vitis vinifera* (Gnanajobitha et al., 2013) and *Carica papaya* (Jain et al., 2009). Here, the fruit rind extract of jackfruit (Figure 1) was used for the eco-friendly synthesis of silver nanoparticles. *Artocarpus heterophyllus* (Jackfruit tree) is well known as the largest tree-borne fruit. It belongs to the mulberry family, *Moraceae*. However, there is no report on using jackfruit rind to prepare silver nanoparticles.

MATERIALS AND METHODS

Preparation of jackfruit rind extract

The whole jackfruit rind was washed several times with distilled water to remove dirt or uncoordinated materials present on the peel. Then, 100 g of jackfruit rind was cut into small pieces, shade dried and powdered. The 50 g of dried powder was boiled in 250 ml of sterile nanopure water in a 500 mL Erlenmeyer flask for 30 min at 80°C to obtain the peel extract followed by filtration (Whatman No. 42) and stored at 4°C in the refrigerator for future experimental use.

Synthesis of silver oxide nanoparticles

For synthesis of silver oxide nanoparticles (Ag_2O NPs), the jackfruit rind extract (10 mL) was added to 90 mL of 1 mM silver nitrate solution in 250-ml Erlenmeyer flasks to form a reaction mixture, and the reaction was performed under ambient conditions. The reaction mixture was observed for color change from light yellow to dark brown and confirmation of silver nanoparticle synthesis is shown in Figure 1. The intensity of the color was measured using a UV-visible spectrophotometer (UV-1800, UV-Vis spectrophotometer, Shimadzu, Kyoto, Japan) within a working wavelength range of 200 to 800 nm using a dual beam operated at 1 nm resolution).

Optimization of Ag_2O NPs productions

To optimize the nanoparticle production, parameters such as pH of 3, 4, 5, 6, 7, 8, 9 and 10, fruit rind extract at various concentrations of 0.5, 1, 1.5, 2, 2.5, 3, 3.5, 4, 4.5 and 5%, Ag^+ at 0.1, 0.2, 0.3, 0.4, 0.5, 0.6, 0.7, 0.8, 0.9 and 1.0 mM concentrations and reaction times of 0, 15, 30, 45, 60, 75, 90, 105, 120, 135, 150, 165, 180, 195, 210, 240, 270 min were tested. Once the silver nanoparticle production was completed, it was centrifuged at 12,000 rpm for 15 min followed by several washes with copious amounts of nanopure water and ethanol to ensure better separation of free entities from the silver nanoparticle. The product was freeze-dried to make a powder and used for further characterization and antifungal studies.

Characterization of Ag_2O NPs

For characterization, Fourier transform infrared (FTIR) spectra of the phytoconstituents and silver nanoparticles were obtained using a Perkin-Elmer FTIR spectrophotometer (Norwalk, CT, USA) in the diffuse reflectance mode at a resolution of 4 particles cm^{-1} in KBr pellets. High resolution-transmission electron microscopy (HR-TEM model, JEOL-2010, Japan) was used to examine the surface morphology and size of the silver nanoparticles. X-ray powder diffraction of the nanoparticle was obtained using a Rigaku X-ray diffractometer (XRD, Rigaku, Japan).

Antifungal activity of Ag_2O NPs against plant pathogenic fungi

The antifungal activity of Ag_2O NPs, bulk metal silver, rind extract,

Ag_2O NPs blend with rind extract, and standard antifungal (nystatin) were determined by a well diffusion method against the plant pathogenic fungi, viz., *Phytophthora capsici* (KACC 40475), *Phytophthora drechsleri* (KACC 40190), *Didymella bryoniae* (KACC 40900), *Colletotrichum acutatum* (KACC 40042) and *Cladosporium fulvum* (KCCM 11466) obtained from Korean Agricultural Culture Collection (KACC) and maintained in a potato dextrose agar (Ingredients Gms/Litre Potatoes, infusion from 200 g/L, Dextrose 20 g/L, Agar 15 g/L, final pH (at 25°C) 5.6±0.2) cultured in potato dextrose agar medium. The agar wells were made using a sterile juice straw with 5 mm distance to the edge of the plate. The wells were impregnated with Ag_2O NPs at concentrations of 20, 40, and 80 µg/well, bulk metal silver (80 µg/well), gum solution (20 µl/well), and Ag_2O NPs blend with extract (20 µl/well). All fungal isolates were individually inoculated on sterile PDA medium with a 6 mm cork borer in two edge of the Petri plate. The antifungal activities of the jackfruit rind extract and the Ag_2O NPs were determined according to Velmurugan et al. (2016).

RESULTS AND DISCUSSION

The jackfruit (*A. heterophyllus*) rind extract mediated silver nanoparticle fabrication was achieved by adding 1 mM silver ion complex ($AgNO_3$). Next, the aqueous solution was slowly reduced with a color change from light yellow to dark brown (Figure 1) over 20 min in room temperature. The presence of silver nanoparticles was confirmed (Chauhan et al., 2011). The surface plasmon was at 428 nm for the room temperature reaction (Kamat et al., 1998; Rani and Rajasekharreddy, 2011; Gnanajobitha et al., 2013). The common silver nanoparticles synthesis depends on nucleation and growth mechanism (Rai et al., 2006; Fayaz et al., 2009; Song and Kim, 2009; Kaviya et al., 2011). *The* UV–Vis spectra for the formation of silver nanoparticles at different pH values are *shown in Figure 2a. The pH plays a key role in nanoparticle formation.* The shape and size of the nanoparticles are dependent on the pH of the solution. In this study, the absorbance band increased while the pH increased from 4 to 9 for silver nanoparticles. A lower and broader absorbance in silver nanoparticles was observed at lower pH values versus higher pH, this could be due to the larger size of the NPs at lower pH. It has been shown that pH affects the shape and size of a nanoparticles and influences the synthetic process used to make silver nanoparticles (Dwivedi and Gopal, 2010; Vanaja et al., 2013). The results suggest that acidic pH suppresses nanoparticles formation due to increased precipitation or agglomeration due to the instability of the nanoparticles (or the lack of a stabilizing agent). Earlier, Velmurugan et al. (2014a) reported that at a lower pH, agglomeration occurs due to the over-nucleation and formation of larger size nanoparticles. Conversely, at a high pH, many nanoparticles with smaller surface areas are present due to the bioavailability of functional groups in the pine gum solution. Figure 2b shows the UV-Vis spectra of the synthesized silver nanoparticles with different concentrations of jackfruit rind extract (1 to 10%) at 2 mM $AgNO_3$. The peak absorbance consistently increased with increases in the jackfruit rind extract (in 50 mL of 2 mM Ag^+ solution) from 1 to 10% (Figure 2b). These results indicate that more reduction was achieved with jackfruit rind extract concentrations of 2 mL. When the jackfruit rind extract concentration increased, fewer silver nanoparticles were reduced as seen in the spectral peaks in Figure 2c. These results corroborate Pal et al. (2007), Kora et al. (2010) and Velmurugan et al. (2014b) who studied gum acacia, gum kondagogu and pine gum, respectively. The silver ion concentrations were also modulated. The maximum peak absorbance (using UV-Vis) was found for 1.0 mM silver ion with good production (Figure 2c). This could be caused by an enhancement in the oxidation of hydroxyl groups by the metal ions (Kora et al., 2010). The highest yield was observed at 180 min (Figure 2d).

FT-IR analysis (Figure 3) of both jackfruit rind powder extract and silver nanoparticles was done from 4000 to 500 cm^{-1} (Basavegowda and Lee, 2013). The FT-IR spectrum of the water extract of jackfruit rind showed absorptions at the following peaks: 3438 cm^{-1} representing the -OH group; 2931 cm^{-1} assigned to the stretching vibration of C-H methyl and methylene bond; 1743 cm^{-1} assigned to the C=O stretching of pectin ester and carboxylic acid; and 1613 cm^{-1} attributed to the C=O stretching of carboxylic acid with intermolecular hydrogen bond. The peaks at 1422, 1058 and 629 cm^{-1} were assigned to symmetric bending of CH_3, -SO3 and C-O stretching of ether groups, respectively. The FTIR spectrum of the Ag_2ONPs synthesized using jackfruit rind extract shows different bands at 3408, 2922, 1613, 1383, 1020 and 610 cm^{-1}. Upon comparing the FTIR spectra of the extract and Ag_2O NPs, there was a shift in the bands of the carbonyl and hydroxyl groups. This indicates that the major bio-molecules from the extract were capped on the Ag_2O NPs surface and shows their characteristic peaks in the IR spectrum of the silver solution.

HR-TEM was used to study the shape and size of the Ag_2O NPs obtained via jackfruit rind extracts. The HR-TEM image (Figure 4a) shows Ag_2O NPs (11.2 to 24.5 nm) with an abundance of roughly spherical Ag_2O NPs. The selected area electron diffraction (SAED) pattern of Ag_2O NPs is shown in Figure 4b. The bright circular rings in the SAED pattern confirm the crystallinity of the Ag_2O NPs prepared from jackfruit. Some of the nanoparticles do not have a smooth surface morphology due the presence of both individual and agglomerated Ag_2O NPs.

The powder X-ray diffraction of the Ag_2O NPs is shown in Figure 4c. This confirms the presence of genuine silver (I) oxide nanoparticles. The XRD spectra confirmed the standard spectra of Ag_2O (JCPDS no. 00-012-0793). Many Bragg reflection peaks were observed at 2θ values of 32.03, 40.01, 55.02, 65.03 and 77.45°. These are indexed to (111), (111), (200), (220), (220) and (222) planes of pure Ag_2O NPs and match that of the standard spectra of silver (JCPDS no.# 00-004-0783), silver (II) oxide (JCPDS no.# 00-012-0793), and silver oxide

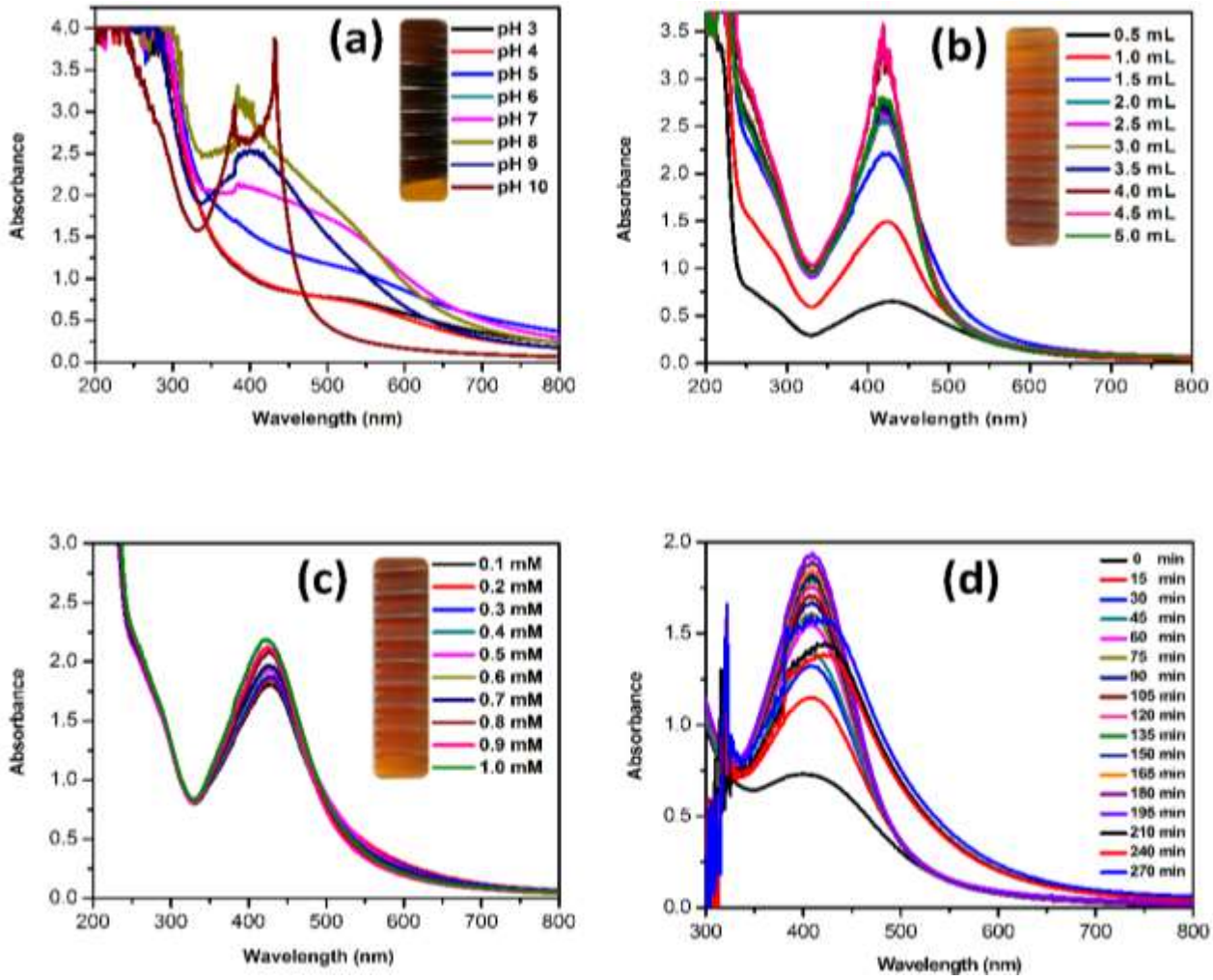

Figure 2. UV–Vis absorption spectra of optimizing parameters to produce Ag_2O NPs with different pHs: (a) ratios of jackfruit rind extract from 0.5 to 5 mL (b), concentration of metal ions Ag^+ from 0.1 to 1.0 mM (c) and times from 0 to 270 min (d).

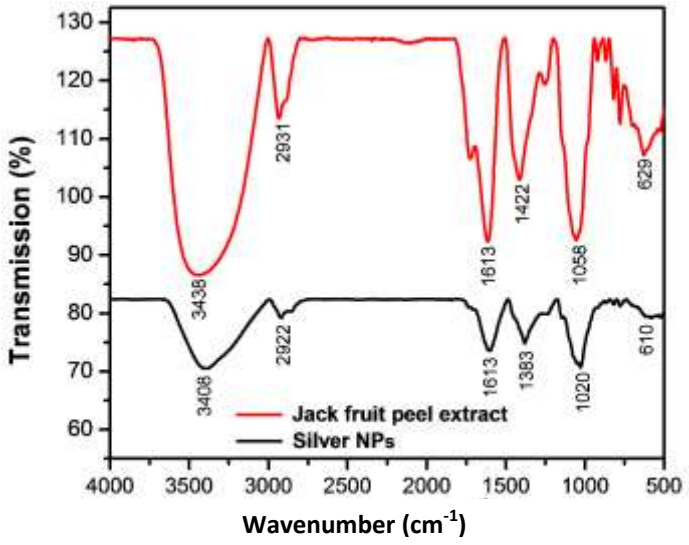

Figure 3. FTIR spectra of the jackfruit rind extract powder and the Ag_2O NPs synthesized at optimum parameters.

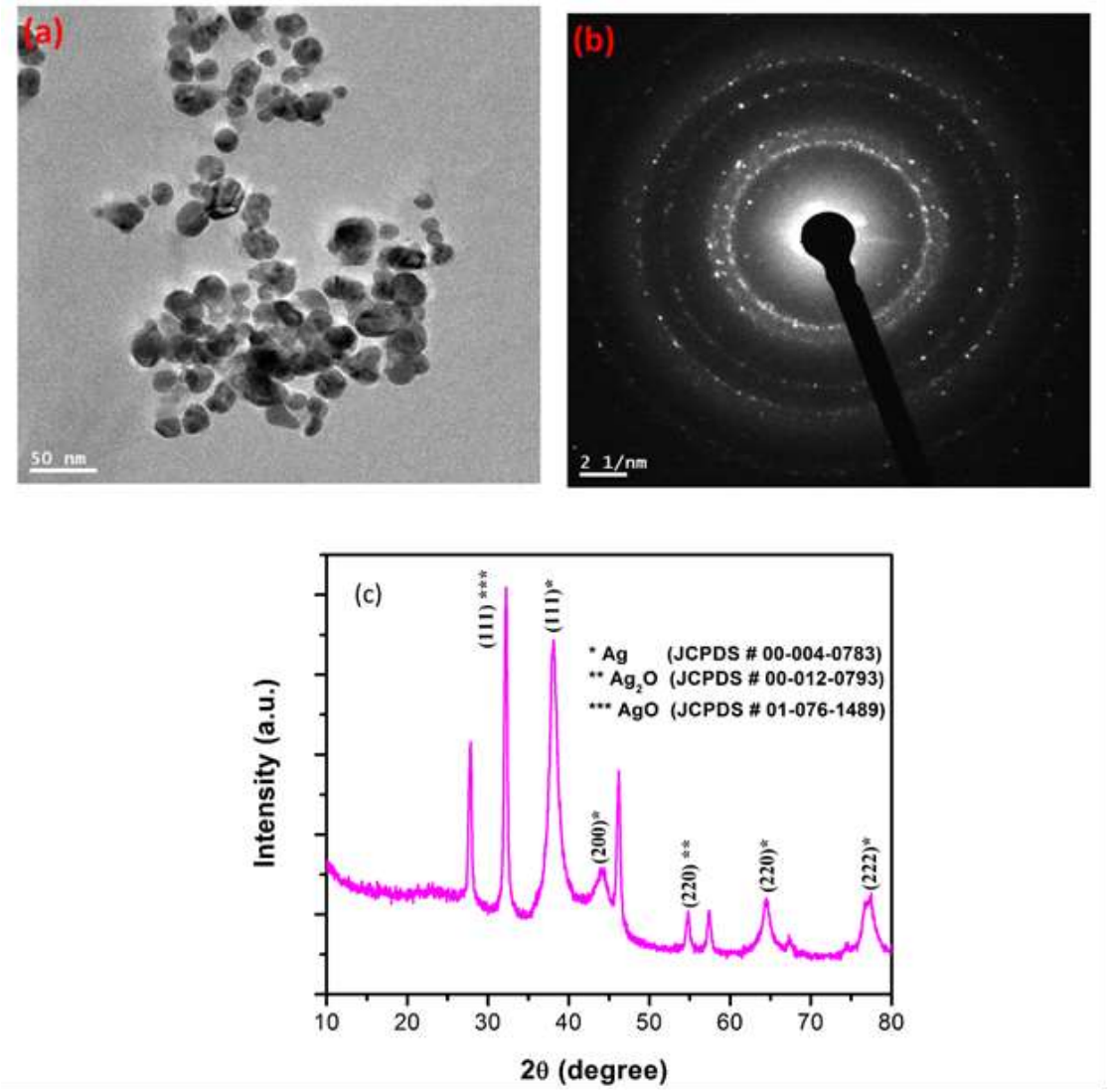

Figure 4. TEM images of Ag_2O NPs (a) 24.2 nm, corresponding SAED pattern for Ag_2O NPs (b) and (c) XRD patterns of the Ag_2O NPs synthesized at the optimum parameters.

(JCPDS no.# 01-076-1489) (Velmurugan et al., 2016). The XRD analysis confirms the face-centered cubic (FCC) configuration of biosynthesized Ag_2O NPs. This used PANalytical X'Pert HighScore Plus software, Version 3.0.3 (Figure 5). The mean particle diameter of Ag_2O NPs was calculated from the XRD pattern using the Scherrer equation:

$D = K\lambda/\beta_{1/2}$ COS θ.

Here, K is the shape constant, λ is the wavelength of the X-ray, $\beta_{1/2}$ and u are the half width of the peak and half of the Bragg's angle, respectively. The calculated average crystallite size of the Ag_2O NPs was 24.2 nm from the breadth of the (111) reflection.

The *in vitro* antifungal activity of synthesized Ag_2O NPs versus a commercially available antifungal agent was carried out for the first time against five different plant pathogenic fungi. The Ag_2O NPs and a combination of extract and Ag_2O NPs showed remarkable activity against four plant pathogenic fungi, *C. acutatum, P. capsici*, *P. drechsleri* and *C. fulvum* (Table 1). The *P. drechsleri* showed resistance to the commercial antifungal agent, nystatin (20 µg/well); however, *D. bryoniae,* were resistant to synthesized Ag_2O NPs (Table1).

Conclusions

In summary, jackfruit rind extract mediated Ag_2O NPs synthesis is a simple technique that contributes to the area of green synthesis and nanotechnology. It has no

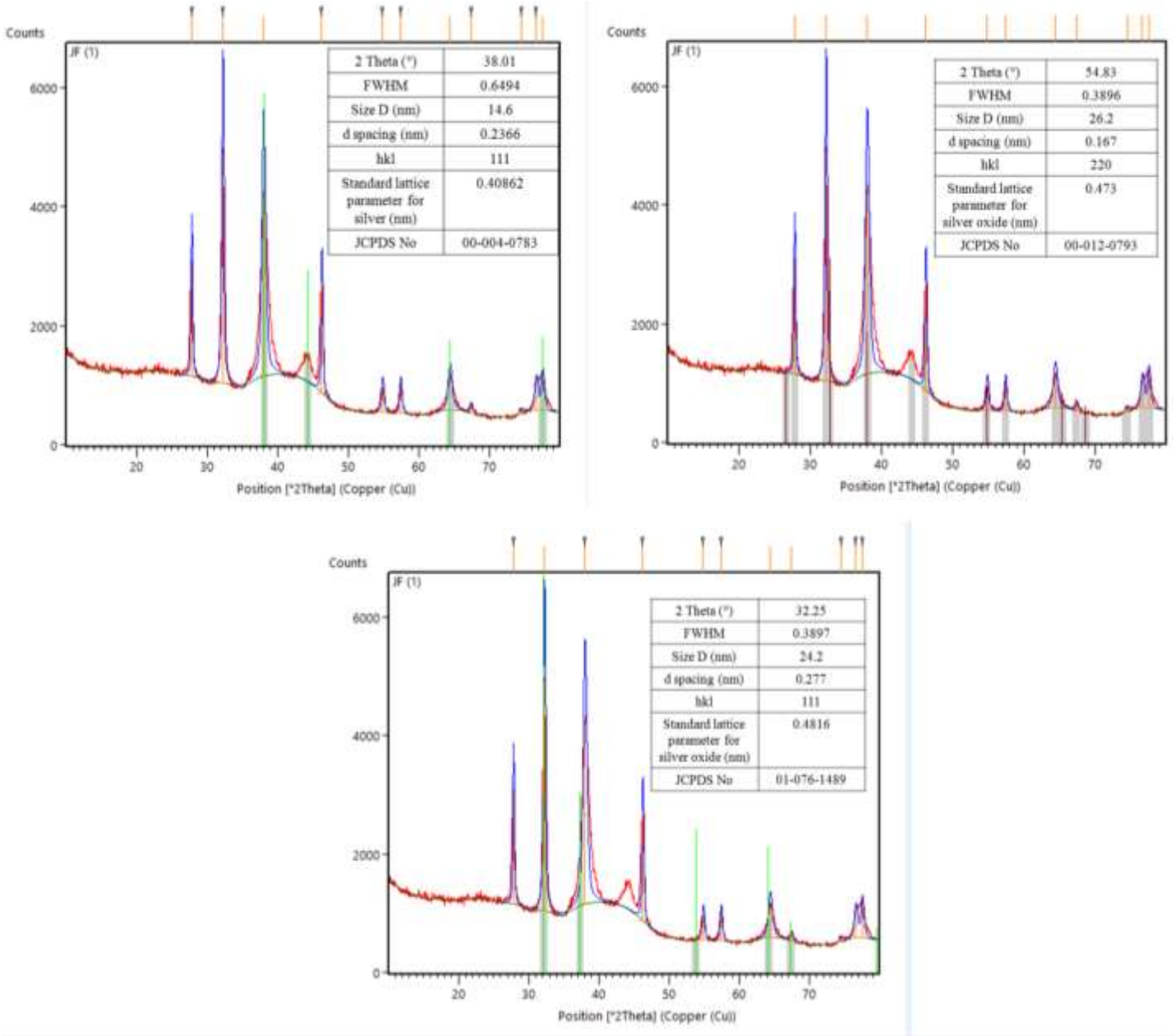

Figure 5. Mean particle diameter of Ag_2O NPs calculated from the XRD pattern using the Scherrer equation.

Table 1. Zone of inhibition (mm) of synthesized Ag_2O NPs and blend of extract with Ag_2O NPs against plant fungal pathogens.

S/N	Strains	Zone of inhibition (ZOI) in mm						
		Ag_2O NPs + extract (µL)			Synthesized Ag_2O NPs (µg)			Control
		25	50	100	100	150	200	
1.	*C. acutatum*	2	4	5	5	8	11	22
2.	*P. capsici*	2	3	6	4	6	8	24
3.	*P. drechsleri*	3	4	6	4	6	10	No zone
4.	*C. fulvum*	2	6	8	8	12	16	22
5.	*D. bryoniae*	No zone	No zone	No zone	No zone	No zone	No zone	24

external chemicals or physical steps. This study showed the efficiency of Ag_2O NPs synthesized by jackfruit rind extracts. This is an environmentally benign method to prepare metal oxide nanoparticles. The product's physical characteristics were analyzed with UV-Vis spectroscopy, FTIR, XRD, techniques and TEM. The Ag_2O NPs were monodisperse, spherical and 10 and 30 nm in diameter. The antifungal activity of Ag_2O NPs was investigated against a plant pathogenic fungus, and it shows moderate to good activity with few pathogens. Based on these findings, this method is suitable for the industrial scale production of Ag_2O NPs from a commonly discarded waste jackfruit rind.

CONFLICT OF INTERESTS

The authors did not declare any conflict of interest.

ACKNOWLEDGEMENT

This work was supported by a 2 Years Research Grant of Pusan National University.

REFERENCES

Bankar A, Joshi B, Kumar AR, Zinjarde S (2010). Banana peel extract mediated synthesis of gold nanoparticles. Colloids Surf. B. 80:45-50.

Basavegowda N, Lee YR (2013). Synthesis of silver nanoparticles using Satsuma mandarin (*Citrus unshiu*) peel extract: A novel approach towards waste utilization. Mater. Lett. 109:31-33.

Chauhan S, Upadhyay MK, Rishi N, Rishi S (2011). Phyto fabrication of silver nanoparticles using pomegranate fruit seeds. Int. J. Nanomater. Biostruct. 1:17-21.

Dubey M, Bhadauria S, Kushwah BS (2009). Green synthesis of nanosilver particles from extract of *Eucalyptus hybrida* (safeda) leaf. Dig. J. Nanomater. Biostruct. 4:537-543.

Dwivedi AD, Gopal K (2010). Biosynthesis of silver and gold nanoparticles using *Chenopodium album* leaf extract. Colloids Surf. A Physicochem. Eng. Asp. 369:27-33.

Fayaz AM, Balaji K, Kalaichelvan PT, Venkatesan R (2009). Fungal based synthesis of silver nanoparticles—an effect of temperature on the size of particles. Colloids Surf. B Biointerfaces 74:123-126.

Gnanajobitha G, Paulkumar K, Vanaja M, Rajeshkumar S, Malarkodi C, Annadurai G, Kannan C (2013). Fruit-mediated synthesis of silver nanoparticles using *Vitis vinifera* and evaluation of their antimicrobial efficacy. J. Nanostructure Chem. 3:67.

Gondwal M, Pant GJN (2013). Biological evaluation and green synthesis of silver nanoparticles using aqueous extract of *Calotropis procera.* Int. J. Pharm. Biol. Sci. 4:635-643.

Jain D, Daima HK, Kachhwaha S, Kothari SL (2009). Synthesis of plant-mediated silver nanoparticles using papaya fruit extract and evaluation of their anti-microbial activities. Dig. J. Nanomater. Biostruct. 4:557-563.

Kamat PV, Flumiani M, Hartland GV (1998). Picosecond dynamics of silver nanoclusters. Photoejection of electrons and fragmentation. J. Phys. Chem. B 102:123-3128.

Kaviya S, Santhanalakshmi J, Viswanathan B, Muthumary J, Srinivasan K (2011). Biosynthesis of silver nanoparticles using citrus sinensis peel extract and its antibacterial activity. Spectrochim. Acta A Mol. Biomol. Spectrosc. 79:594-598.

Kim SW, Jung JH, Lamsal K, Kim YS, Min JS, Lee YS (2012). Antifungal effects of silver nanoparticles (AgNPs) against various plant pathogenic fungi. Mycobiology 40:53-58.

Kora AJ, Sashidhar RB, Arunachalam J (2010). Gum kondagogu (*Cochlospermum gossypium*): a template for the green synthesis and stabilization of silver nanoparticles with antibacterial application. Carbohydr. Polym. 82:670-679.

Lamsal K, Kim SW, Jung JH, Kim YS, Kim KS, Lee YS (2011). Application of silver nanoparticles for the control of *Colletotrichum* species *in vitro* and pepper anthracnose disease in field. Mycobiology 39:194-199.

Lee JH, Lim JM, Velmurugan P, Park YJ, Park YJ, Bang KS, Oh BT (2016). Photobiologic-mediated fabrication of silver nanoparticles with antibacterial activity. J. Photochem. Photobiol. 162:93-99.

Mariselvam R, Ranjitsingh AJA, Nanthini AUR, Kalirajan K, Padmalatha C, Selvakumar PM (2014). Green synthesis of silver nanoparticles from the extract of the inflorescence of *Cocos nucifera* (Family: *Arecaceae*) for enhanced antibacterial activity. Spectrochim. Acta Mol. Biomol. Spectrosc. 129:537-541.

Nazeruddin GM, Prasad NR, Waghmare SR, Garadkar KM, Mulla IS (2014). Extracellular biosynthesis of silver nanoparticle using *Azadirachta indica* leaf extract and its anti-microbial activity. J. Alloys Compd. 583:272-277.

Pal S, Tak YK, Song JM (2007). Does the antibacterial activity of silver nanoparticles depend on the shape of the nanoparticle? A study of the gram-negative bacterium *Escherichia coli.* Appl. Environ. Microbiol. 73:1712-1720.

Rai A, Singh A, Ahmad A, Sastry M, (2006). Role of halide ions and temperature on the morphology of biologically synthesized gold nanotriangles. Langmuir 22:736-741.

Rani PU, Rajasekharreddy P (2011). Green synthesis of silver-protein (core–shell) nanoparticles using *Piper betle* L. leaf extract and its ecotoxicological studies on *Daphnia magna.* Colloids Surf. A Physicochem. Eng. Asp. 389:188-194.

Sadeghi B, Rostami A, Momeni SS (2015). Facile green synthesis of silver nanoparticles using seed aqueous extract of *Pistacia atlantica* and its antibacterial activity. Spectrochim. Acta Mol. Biomol. Spectrosc. 134:326-332.

Song JY, Kim BS (2009). Rapid biological synthesis of silver nanoparticles using plant leaf extracts. Bioprocess Biosyst. Eng. 32:79-84.

Vanaja M, Rajeshkumar S, Paulkumar K, Gnanajobitha G, Malarkodi C, Annadurai G (2013). Phytosynthesis and characterization of silver nanoparticles using stem extract of *Coleus aromaticus.* Int. J. Mater. Biomater. Appl. 3:1-4.

Velmurugan P, Lee SM, Cho M, Park JH, Seo SK, Myung H, Bang KS, Oh BT (2014 a). Antibacterial activity of silver nanoparticle-coated fabric and leather against odor and skin infection causing bacteria. Appl. Microbiol. Biotechnol. 98:8179-8189.

Velmurugan P, Cho M, Lee SM, Park JH, Bae S, Oh BT (2014b). Antimicrobial fabrication of cotton fabric and leather using green-synthesized nanosilver. Carbohydr. Polym. 106:319-325.

Velmurugan P, Shim J, Kim K, Oh BT (2016). *Prunus*× *yedoensis* tree gum mediated synthesis of platinum nanoparticles with antifungal activity against phytopathogens. Mater. Lett. 174:61-65.

academicJournals

Vol. 16(36), pp. 1826-1831, 6 September, 2017
DOI: 10.5897/AJB2017.16130
Article Number: 9D59F1665879
ISSN 1684-5315

http://www.academicjournals.org/AJB

African Journal of Biotechnology

Full Length Research Paper

Phylogenetic characterization of *East African cassava mosaic begomovirus* (*Geminiviridae*) isolated from *Manihot carthaginensis* subsp. *glaziovii* (Müll.Arg.) Allem., from a non-cassava growing region in Tanzania

F. Tairo[1*], W. K. Mbewe[2,3], D. Mark[1], M. Lupembe[1], P. Sseruwagi[1] and J. Ndunguru[1]

[1]Mikocheni Agricultural Research Institute, P.O Box 6226, Dar es Salaam, Tanzania.
[2]School of Agricultural Sciences, Makerere University, P. O. Box 7062, Kampala, Uganda.
[3]Bvumbwe Agricultural Research Station, P. O. Box 5748, Limbe, Malawi.

Received 30 June, 2017; Accepted 9 August, 2017

***Manihot carthaginensis* subsp. *glaziovii* (Müll.Arg.) Allem., a wild relative of cassava, native to Brazil, is one of the popular agroforestry trees used for hedges and/or boundary plants surrounding homesteads and farms and also harbours cassava mosaic begomoviruses (CMBs) and cassava brown streak ipomoviruses. Sequences of the DNA-A component of *East African cassava mosaic virus* (EACMV) isolates from *M. carthaginensis* subsp. *glaziovii* (Müll.Arg.) Allem., collected from non-cassava growing areas of Tanzania were characterized. Thirteen full length DNA-A sequences were analysed together with 15 already reported EACMV sequences and six CMB species reference genomes. The results show 96 to 100% nucleotide sequence identity with EACMV isolates from Kenya. Phylogenetic analysis revealed that EACMV isolates from *M. carthaginensis* subsp. *glaziovii (*Müll.Arg.) Allem, belong to a single cassava mosaic begomovirus species. The EACMV monophyletic clade is distinct from all other CMB species. The presence of Cassava infecting begomoviruses in wild cassava relative growing from traditionally non cassava growing region serve as inoculum sources for cassava-infecting begomoviruses and therefore their eradication is key in the sustainable management of CMBs, especially in the non-cassava growing areas.**

Key words: Cassava mosaic disease, East African cassava mosaic virus, *Manihot carthaginensis* subsp. *glaziovii* (Müll.Arg.) Allem., genetic diversity.

INTRODUCTION

Manihot carthaginensis subsp. *glaziovii* (Müll.Arg.) Allem., commonly called 'tree cassava plays a crucial role in cassava improvement programs as the source of disease resistance, particularly for cassava mosaic disease (CMD) and cassava brown streak disease (CBSD) (Nichols, 1947). In traditional cassava growing areas, it provides

*Corresponding author: E-mail: fredtairo@gmail.com.

cheap source vegetable while in non-cassava producing areas, it is one of the popular agroforestry trees used for hedge/or boundary plants surrounding homesteads and farms; it is also used in small quantities for animal fodder. However, despite its crucial roles, it is also responsible for the perpetuation of CMD and CBSD in traditional cassava growing areas and non-growing areas.

Several studies on the epidemiology of CMD have established a potential role of non-cassava plant species as alternate reservoir in perpetuation of CMBs (Alabi et al., 2008). However, these studies have revealed occurrence of at least three CMBs species in wild relative and weed plants, and each study focused primarily on traditional cassava growing areas. In Nigeria, both *African cassava mosaic virus* (ACMV) and *East African cassava mosaic virus* (EACMV) were reported in *M. carthaginensis* subsp. *glaziovii* (Müll.Arg.) Allem., and leguminous plants and in *Leucaena leucocepohala* (Alabi et al., 2008). But most of these studies have concentrated on traditional cassava growing areas where the interaction of cassava and its wild relatives and/or weeds is common. While some information is available on the natural occurrence of EACMV (Ogbe et al., 2006) in *Manihot* spp., little is known about the occurrence of cassava mosaic like symptoms in *M. carthaginensis* subsp*. glaziovii* (Müll.Arg.) Allem*.,* in the traditional non-cassava growing areas.

Kilimanjaro region in northern Tanzania is a traditional non cassava growing region, where *M. carthaginensis* subsp*. glaziovii* (Müll.Arg.) Allem., is a popular agroforestry tree used as a hedge/or border plant-surrounding banana and coffee fields. Significant part of the region is in lower land with favourable climate for commercial cassava production. Thus, understanding the status of CMD and the diversity of associated viruses is worth studying in order to devise a sustainable measure to eradicate the inoculum and a measure for the CMD sources. In this study, a total of 13 CMB DNA-A sequences from *M. carthaginensis* subsp*. glaziovii* (Müll.Arg.) Allem., sampled from non-cassava growing farmer fields in Kilimanjaro, Tanzania were characterized to investigate their identity and diversity in relation to corresponding DNA-A sequences.

MATERIALS AND METHODS

M. carthaginensis subsp. *glaziovii* (Müll.Arg.) Allem., leaf samples displaying cassava mosaic like symptoms ranging from mild chlorotic mosaic to severely distorted leaf and filform (Figure 2) were collected in 3 districts: Moshi rural, Rombo and Siha (Figure 1). Total DNA was extracted from leaves stored in a silica gel as described (Alabi et al., 2008) and used as a template for rolling-circle amplification (RCA) of complete begomovirus genomes as per Illustra TempliPhi amplification kit (GE Healthcare Life Sciences, UK). The RCA products were first PCR-amplified using begomovirus universal primer pair EBB555F /R1 (Fondong et al., 2000) to see if they contain any begomovirus infection, and subsequently used to construct Illumina libraries and sequenced at North Carolina State Genomic Sciences Laboratory (Raleigh, NC, USA) by next generation sequencing.

Raw reads for each sample were assembled using *de novo* assembly tool on CLC Genomics Workbench, mapped and aligned using reference sequences obtained from GenBank (Table 1 and Figure 3) representing full length DNA-A component of cassava begomoviruses under the following conditions: minimum overlap (10%), minimum overlap identity (80%), allow gaps (10%) and fine tuning set to iterate up to 10 times.

Nucleotide sequence identities were computed using sequence demarcation tool (SDT) version 1.2 (Muhire et al., 2014). The identity scores were calculated as 1-(M/N) where M is the number of mismatching nucleotides and N the total number of positions along the alignment at which neither sequence has a gap (Muhire et al., 2014). Multiple sequence alignments of the full length DNA-A component determined from *M. carthaginensis* subsp*. glaziovii* (Müll.Arg.) Allem., were generated using the Clustal W alignment function in Mega 7 (Kumar et al., 2016) and edited visually. Same MEGA 7 was used to construct maximum-likelihood (ML) phylogenetic trees. Initial trees for the heuristic search were obtained automatically by applying Neighbor-Joining algorithm (Tamura et al., 2004) to a matrix of pairwise distances estimated using the maximum composite likelihood approach, and then selecting the topology with superior log likelihood value (Kumar et al., 2016). All positions containing gaps and missing data were eliminated. Evolutionary analyses were conducted in MEGA7 (Kumar et al., 2016). The General Time Reversible (GTR) nucleotide substitution model was used (selected as the most appropriate by ML). The stability of the inferred branches was estimated by bootstrapping with 1000 replicates.

RESULTS AND DISCUSSION

PCR screening using begomovirus universal primer pair (Fondong et al., 2000) amplified expected fragments of 552 bp both in symptomatic and non-symptomatic samples indicating they were singly infected with begomovirus species. The next generation sequencing reads of 38 samples produced a pired sequences data of 7,247,392.00 million reads. After trimming for non-viral sequences 7,151,881 million reads remained and were assembled *de novo* to a total of 40 contigs. Subsequent Blast search of the assembled contigs identified 23 contigs ranging from 201 to 620 nt in length with average of 411 nt with respect to reference sequences in the GenBank from which 13 full length sequences (2,800 nts) corresponding to DNA A were obtained. The resulting nucleotide sequences were deposited in GenBank under accession numbers MF067253-MF067265 (Table 1).

Pairwise comparison of full-length sequences of DNA-A molecules with available sequences in GenBank suggested all the sequences are related to EACMV Kenyan isolates (Figure 3). The DNA-A sequences were the most similar (97 to 100% nt sequences identity) to EACMV-Kenyan isolates as compared to DNA-B with 92 to 100% nt sequence identity. Based on begomovirus thresholds for species demarcation (Brown et al., 2015), a phylogenetic tree based on the DNA-A component sequences demonstrated a close genetic relationship among EACMV isolated from *M. carthaginensis* subsp*. glaziovii* (Müll.Arg.) Allem., in this study with EACMV Kenyan isolates (Figure 3).

A phylogenetic tree constructed using all 13 DNA-A full

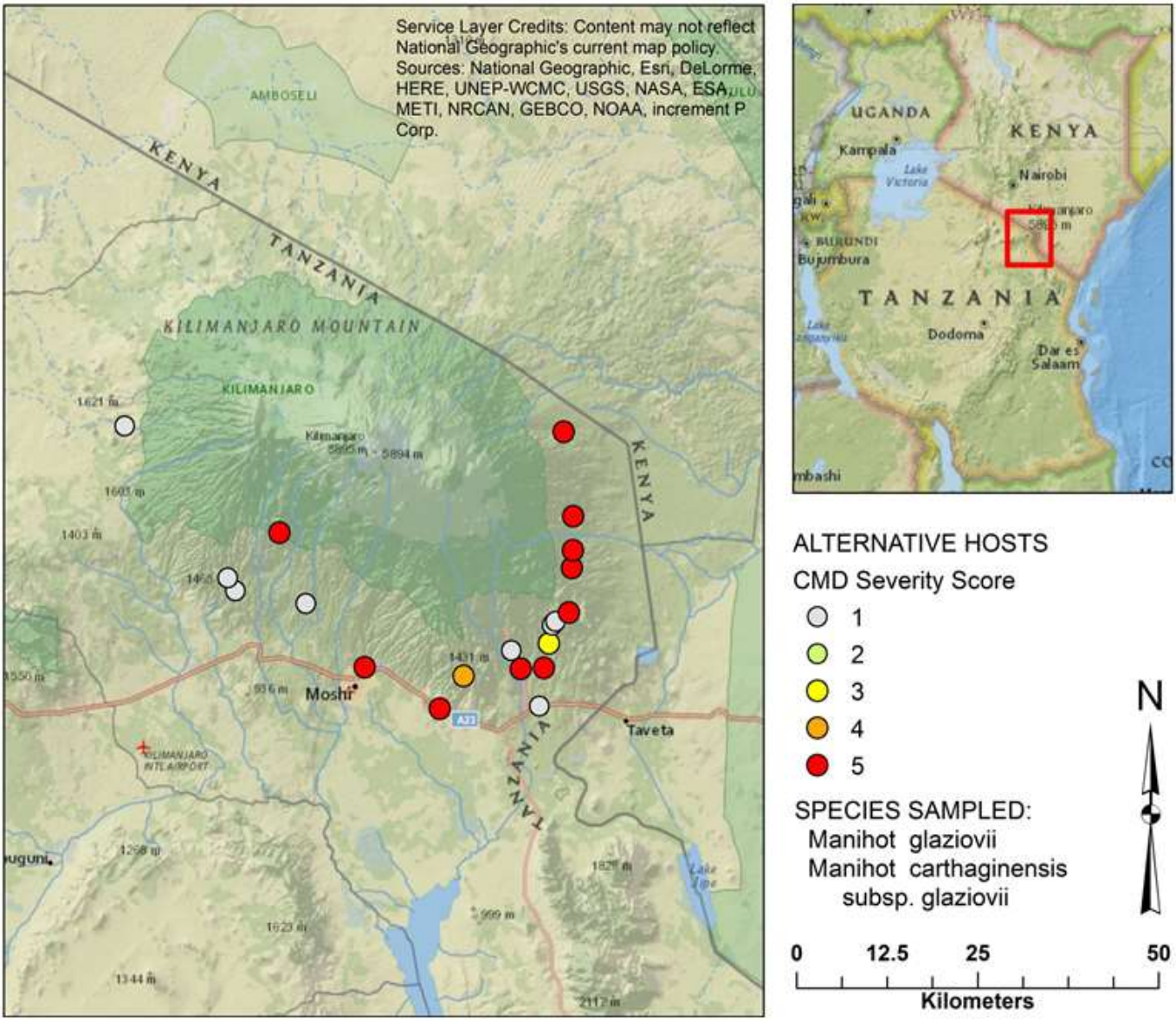

Figure 1. Map of Tanzania showing sampling areas.

length sequences and those available in the GenBank revealed at least two major clusters, with the second cluster having at least four monophyletic clades (Figure 3). This result suggests that although all the EACMV isolates from *M. carthaginensis* subsp. *glaziovii* (Müll.Arg.) Allem. in this study clustered in at least four different clades, there is a still high level of similarity with nucleotide sequence identity between clades, with high similarity in the nucleotide sequence identity of 98 and 99%.. Search for any evidence of recombination among the sequences of full length DNA-A components isolated in this study using RDP4 analysis revealed no evidence of any recombination event.

CMD is a serious problem in SSA, especially in a traditional cassava growing regions, where CMD inoculums and whitefly (*Bemisia tabaci*) vector populations appear to be high throughout the year. Identification of EACMV in *M. carthaginensis* subsp. *glaziovii* (Müll.Arg.) Allem. in three districts in the slope of Mt. Kilimanjaro around 1,573 m above sea level in Tanzania shows CMB inoculum is already present in the region ahead of cassava cultivation. Thus, earlier reports on the factors influencing perpetuation of CMD were confirmed (De Bruyn et al., 2016). Analysis of nucleotide sequences of full length DNA-A and absence of recombination among the determined sequences showed that only one species of CMB is restricted within the surveyed districts with possible introduction from the nearby country (Figures 1

Figure 2. A, *M. carthaginensis* subsp. *glaziovii* (Müll.Arg.) Allem., growing in homesteads as shade trees. **B**, leaves with CMD-like symptoms. **C** and **E**, border surrounding a banana field. **D,** healthy plant along the road.

Table 1. Cassava mosaic begomovirus sequences used in the analysis.

Isolate name	Component	Location name	Accession number
EACMV-TZ_Kch:Mg4:17	DNA-A	Kichui Mwika, Moshi rural	MF067253
EACMV-TZ_Kih:Mg5:17	DNA-A	Kilacha Himo, Moshi rural	MF067254
EACMV-TZ_Krm:Mg11:17	DNA-A	Kirueni Mwika, Moshi rural	MF067255
EACMV-TZ_Krm:Mg12:17	DNA-A	Kirueni Mwika, Moshi rural	MF067256
EACMV-TZ_Krm:Mg13:17	DNA-A	Kirueni Mwika, Moshi rural	MF067257
EACMV-TZ_Kel:Mg17:17	DNA-A	Kilamfua, Rombo	MF067258
EACMV-TZ_Sh:Mg24:17	DNA-A	Shimbi, Rombo	MF067259
EACMV-TZ_Kim:Mg25:17	DNA-A	Kimangaro Mwika, Moshi rural	MF067260
EACMV-TZ_Mas:Mg30:17	DNA-A	Masama Tema, Siha	MF067261
EACMV-TZ_Mas:Mg31:17	DNA-A	Masama Tema, Siha	MF067262
EACMV-TZ_Kan:Mg35:17	DNA-A	Kangeri Mashati, Rombo	MF067263
EACMV-TZ_Eng:Mg38:	DNA-A	Engarenairobi Sanyajuu, Siha	MF067264
EACMV-TZ_Man:Mg1:17	DNA-A	Mansera Sokoni, Rombo	MF067265
EACMV-K29	DNA-A	Kwale Kibaoni, Kenya	AJ717551
EACMV-K312	DNA-A	Machakos Migwani, Kenya	AJ717547
EACMV-K322	DNA-A	Kwale kibaoni, Kenya	AJ717556
EACMV-K325	DNA-A	Kitui Township, Kenya	AJ717548
EACMV-K313	DNA-A	Machakos Migwani, Kenya	AJ717549
EACMMV	DNA-A	Malawi	AJ006460
EACMKV	DNA-A	Machakos,Kenya	AJ717571
EACMZV	DNA-A	Kwale Msambweni, Kenya	AJ717568
EACMV	DNA-A	Uganda	AF126806

Table 1. Contd.

EACMV-UG	DNA-A	Uganda	FN668377
SACMV	DNA-A	South Africa	AF1558061
CMMGV	DNA-A	Toliary, Madagascar	HE617300
ACMV	DNA-A	Pwani,Tanzania	AY795982
SLCMV	DNA-A	Kerala, India	AJ890226
ICMV	DNA-A	Kerala, India	AJ575820

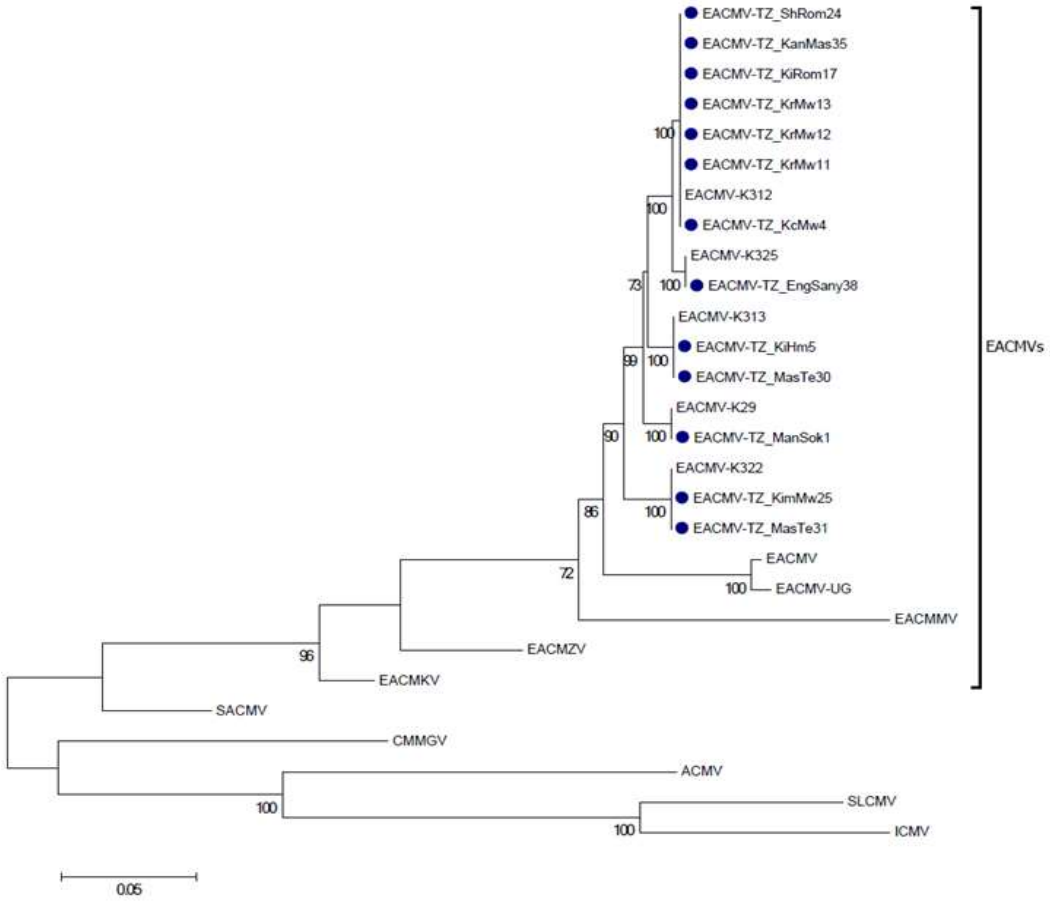

Figure 3. A ML phylogenetic tree of the complete sequences of EACMV-DNA-A isolated from *M. carthaginensis* subsp. *glaziovii* (Müll.Arg.) Allem., in Tanzania. Numbers in branches represent bootstrap values of 1000 replicates (shown only when >70%) and scale bar indicates nucleotide substitutions per site. The EACMV virus sequenced sequenced from *M. carthaginensis* subsp.*glaziovii* (Müll.Arg.) Allem., host in this study are shown in blue and abbreviated as Mg; EACMV[TZ:Kch:Mg4:17] *East African cassava mosaic virus* [Tanzania:Kichuimwika:2017], EACMV[TZ:Kih:Mg5:17] *East African cassava mosaic virus* [Tanzania:KilachaHimo:2017], EACMV[TZ:Krm:Mg11:17] *East African cassava mosaic virus* [Tanzania:KirueniMwika:2017], EACMV[TZ:Krm:Mg12:17] *East African cassava mosaic virus [Tanzania:*Kiruenimwika:2017], EACMV[TZ:Krm:Mg13:17] *East African cassava mosaic virus* [Tanzania:Kiruenimwika:2017], EACMV[TZ:Kel:Mg17:17], *East African cassava mosaic virus* [Tanzania:Kelamfuarombo:2017], EACMV[TZ:Shi:Mg24:17], *East African cassava mosaic virus* [Tanzania:Shimbirombo:2017], EACMV[TZ:Kim:Mg25:17] *East African cassava mosaic virus* [Tanzania:Kimangaro:2017], EACMV[TZ:Mas:Mg30:17] *East African cassava mosaic virus [Tanzania:*Masama:2017], EACMV[TZ:Mas:Mg31:17] *East African cassava mosaic virus* [Tanzania:Masama:2017] EACMV[TZ:Kan:Mg35:17] *East African cassava mosaic virus* [Tanzania:KangeriMashati:2017], EACMV[TZ:Eng:Mg38:17] *East African cassava mosaic virus* [Tanzania:Engarenairobi:2017], EACMV[TZ:Mam:Mg1:17], *East African cassava mosaic virus* [Tanzania:Mamsera:2017], EACMV-[K29] *East African cassava mosaic virus* [Kenya:K29], EACMV[K312] *East African cassava mosaic virus* [Kenya:K312], EACMV[K322] *East African cassava mosaic virus* [Kenya:K322], *East* EACMV[K325] *African cassava mosaic virus* [Kenya:K325], EACMV[K313] *East African cassava mosaic virus* [Kenya[K313]. Naming of isolates is based on Brown et al. (2015).

and 3), and continues to spread through use of infected cuttings. Since *M. carthaginensis* subsp. *glaziovii* (Müll.Arg.) Allem. in Kilimanjaro region is an important agroforestry tree, there is a need to creat awareness on its role in introducing and spreading cassava mosaic begomoviruses and cassava brown streak viruses. There is no doubt that continuous use of virus-infected *M. carthaginensis* subsp. *glaziovii* (Müll.Arg.) Allem., as hedge/or border plants guarantees the most efficient virus inoculum reservoir for introduction of CMD into cassava once introduced in the region. The findings form the basis for strategic management and possible eradication of the CMD-affected plants of M. *carthaginensis* subsp. *glaziovii* (Müll.Arg.) Allem., as inoculum sources. This may be achieved through conducting aggressive awareness campaigns to educate farmers on CMD epidemiology coupled with eradication of all plants with CMD-like symptoms to limit further spread of CMD. It is therefore recommended that, given availability of resources, cassava viral disease surveillance should not be limited to traditionally cassava growing regions only.

CONFLICT OF INTERESTS

The authors have not declared any conflict of interests.

ACKNOWLEDGEMENTS

This study was funded by the “Bill & Melinda Gates Foundation” (Grant no. 51466) to Mikocheni Agricultural Research Institute (MARI) through the “Disease diagnostics for sustainable cassava productivity in Africa” project. The authors acknowledge the assistance of Dr. Anna Szyniszewska of Rothamsted Research Institute, United Kingdom for her assistance in generating survey map.

REFERENCES

Alabi OJ, Ogbe FO, Bandyopadhyay R, Kumar PL, Dixon AGO, Hughes JD'A, Naidu RA (2008). Alternate hosts of African cassava mosaic virus and East African cassava mosaic Cameroon virus in Nigeria Arch. Virol. 153:1743-1747.

Brown J, Zerbini FM, Navas-Castillo J, Moriones E, Ramos-Sobrinho R, Silva JF, Fiallo-Olivé E, Briddon R, Hernández-Zepeda C, Idris A, Malathi VG, Martin D, Rivera-Bustamante R, Ueda S, Varsani A (2015). Revision of *Begomovirus* taxonomy based on pairwise sequence comparisons. Arch. Virol. 160:1593-1619.

De Bruyn A, Harimalala M, Zinga I, Mabvakure BM, Hoareau M, Ravigne V, Walters M, Reynaud B, Varsani A, Harkins GW, Martin DP, Lett J, Lefeuvre P (2016). Divergent evolutionary and epidemiological dynamics of cassava mosaic geminiviruses in Madagascar. BioMed. Cent. 16:182.

Fondong VN, Pita JS, Rey MEC, De kochko A, Beachy RN, Fauquet CM (2000). Evidence of synergism between African cassava mosaic virus and the new double recombinant geminivirus infecting cassava in Cameroon. J. Gen. Virol. 81:287-297.

Kumar S, Stecher G, Tamura K (2016). Molecular Genetics Analysis version 7.0 for bigger data sets. Mol. Biol. Evol. 33:1870-1874.

Muhire BM, Varsani A, Martin DP (2014). SDT: A Virus Classification Tool Based on Pairwise Sequence Alignment and Identity Calculation. PLoS ONE 9(9):e108277.

Nichols RFJ (1947). Breeding cassava for virus resistance. East Afr. Agric. J. 12:184-194.

Ogbe FO, Dixon AGO, Hughes Jd'A, Alabi OJ, Okechukwu R (2006). Status of cassava begomovirus and their new natural hosts in Nigeria. Plant Dis. 90:548-553.

Tamura K, Nei M, Kumar S (2004). Prospects for inferring very large phylogenies by using the neighbor-joining method. Proc. Natl. Acad. Sci. USA 101:11030-11035.

academicJournals

Vol. 16(36), pp. 1832-1839, 6 September, 2017
DOI: 10.5897/AJB2017.16090
Article Number: D0304ED65883
ISSN 1684-5315

http://www.academicjournals.org/AJB

African Journal of Biotechnology

Full Length Research Paper

Genetic diversity of Cameroonian bread wheat (*Triticum aestivum* L.) cultivars revealed by microsatellite markers

Honoré Tékeu[3], Eddy M. L. Ngonkeu[1,3], François P. Djocgoué[3], Aletta Ellis[2], Venasius Lendzemo[1], Lezaan Springfield[2], Lionel Moulin[5], Agnieszka Klonowska[5], Diégane Diouf[4], Willem C. Botes[2]* and Gilles Béna[5]

[1]Institute of Agricultural Research for Development, P. O. Box 2123, Yaoundé, Cameroon.
[2]Department of Genetics, Stellenbosch University, Private Bag X1, Matieland, Stellenbosch, 7602, South Africa.
[3]Department of Plant Biology, Faculty of Science, University of Yaoundé I, P. O. Box 812, Yaoundé, Cameroon.
[4]Laboratoire Commun de Microbiologie de Dakar, Centre de recherche IRD/ISRA/UCAD, Route des Hydrocarbures, Bel Air, P. O. Box 1386, Dakar, Sénégal.
[5]IRD, CIRAD, Laboratoire des Interactions Plantes-Microorganismes-Environnement (IPME), Université de Montpellier, 911 Avenue Agropolis 34394 Montpellier, France.

Received 29 May, 2017; Accepted 4 August, 2017

The assessment of genetic diversity is a key prerequisite for studying the adaptation of populations to new environmental conditions, and therefore for the selection of new varieties. The present investigation aimed to estimate the levels and genetic structure within bread wheat varieties grown in Cameroon. Thus, genetic diversity was assessed in 17 hexaploid wheat cultivars, using 11 microsatellite markers. Genetic resources were collected in the Northwest, Adamawa and North Regions. All pairs of specific marker loci used gave amplifications with allelic variations of size on all DNA of wheat accessions. A total of 77 alleles were detected among cultivars and the number of alleles per locus ranged from 2 to 13 with an average of 7, comparable to those observed in most previous studies. Gene diversity ranged from 0.46 (Xgdm 125) to 0.90 (Xgwm 177) with an average of 0.88, increasing with the number of alleles, with a correlation coefficient of 0.88 (Adamawa) and 0.76 (Northwest). Microsatellite markers used had an average value of polymorphic information content (PIC) of 0.69, indicating that these markers are highly informative in this study. These markers are valid and will make a contribution to the studies in hexaploid wheat. Moreover, cluster analysis at a genetic similarity of 80% and the principal component analysis, where the first two components explaining 59.86% of variation which structured 17 accessions in 5 main distinct groups. This high diversity revealed among wheat accessions, grown in Cameroon could be used in the breeding programs.

Key words: Genetic diversity, bread wheat (*Triticum aestivum* L.), simple sequence repeats (SSR), Cameroon.

INTRODUCTION

The global demand for wheat yields has been estimated to increase by 50% in 2050, in order to feed the world's

growing population (Grassini et al., 2013; Allen et al., 2017). To meet this demand, wheat production should be increased through agricultural intensification in cropping regions areas. To this end, Rajaram and Hettel (1994) had delimited 12 Mega environments (MEs) for wheat cultivation, where three correspond to several agroecological areas in Cameroon. Among them, the main Cameroonian areas are in the North, North-West and Adamawa Regions.

Wheat production is a means of subsistence for many families in Cameroon. Indeed, the cultivation of wheat has started in Cameroon since 1975, through the Development Society for the Cultivation and Processing of Wheat (SODEBLE). Located in Wassandé (Adamawa's Region), the SODEBLE has grown wheat, converted wheat into flour, marketed and carried trials, in order to improve the production technics. Before its closure, this Company had produced high yielding wheat lines resistant to major fungal diseases (Monthé Biris and Habas, 1980). Twelve of these bread wheat varieties were evaluated for the agronomic traits in the North-West Region (Ayuk-Takem, 1984).

In addition, Ayuk-takem (1984) evaluated the agronomic characteristics of 12 varieties of bread wheat in the Northwest Region to identify high yielding varieties for Bui and other agro-ecological zones in high altitudes in Cameroon. The study showed that the local variety (IRAB-1) had the highest yield (4.1 t/ha), but with a non-significant difference with the varieties Chris Mutageneuse (3.5t/ha) and wheat Blésil 430 (4 t/ha). However, the yields of these three varieties were significantly better compared to all other tested varieties. These varieties had also been subjected to various agronomic tests in 1985/1986. In doing so, certain varieties had not been made available to Cameroonian farmers. Until today, beyond these agronomic evaluations, no studies have ever been carried out on the genetic variability of wheat cultivars grown in Cameroon.

Evaluating the genetic diversity is a prerequisite for studying the adaptation of populations to new environmental conditions and hence for the selection of new varieties. The loss of genetic diversity due to modern breeding practices has been reported in several studies (Fu et al., 2005). Several authors have shown that the narrowness of crop genetic diversity could lead to increased susceptibility to diseases and pests, as well as the inability of plants to respond to different environmental constraints (Gorji and Zolnoori, 2011). Therefore, it is necessary to estimate the level of genetic diversity within existing varieties to serve as a base for strategies development geared in the management and exploitation of genetic resources.

In this context, the use of molecular markers to assess genetic diversity is necessary because, unlike phenotypic markers, they are independent from environmental effects (Reza et al., 2015). Several markers, independently or in combination with others, were efficiently used for wheat genetic diversity analyses, including morphological traits (Sonmezoglu et al., 2012). Randomly amplified polymorphic DNAs (RAPDs) (Mukhtar et al., 2002), amplified fragment length polymorphisms (AFLPs) (Reza et al., 2015), restriction fragment length polymorphism (RFLPs) (Bohn et al., 1999) and diversity array technology (DArT) markers have recently been developed and used for genetic diversity assessment and mapping (Ryan et al., 2009), as well as Single nucleotide polymorphisms (SNPs) (Froese and Carter, 2016).

On the other hand, the use of simple sequence repeats (SSRs) markers combines with many desirable marker properties such as abundance, high levels of polymorphism (unlike RFLP), very good reproducibility (compared to RAPD), and co-dominance (contrary to the AFLP for which codominance is not exploitable), but also an even coverage of the genome and the specificity of amplification. In wheat, SSRs markers have been used successfully in a wide range of applications such as genotype identification (Prasad et al., 2000), diversity studies (Akfirat and Uncuoglu, 2013) and genetic mapping. This present study aimed to assess the level of genetic diversity of bread wheat accessions grown in Cameroon.

MATERIALS AND METHODS

Plant material and genomic DNA extraction

The plant material consists of 17 cultivars of bread wheat (*Triticum aestivum* L.) collected in six villages located in two Regions of Cameroon (Table 1). Among them, 11 accessions were collected in five villages of Northwest and 6 were collected from one village (Wassande) of Adamawa region. The cultivars of the North West are mainly local seeds, whereas those of Adamawa were originally given by the SODEBLE and some others were imported from Tchad. In our study, we collected all materials used by farmers in those regions.

An adjusted Doyle and Doyle (1990) protocol was used to extract genomic DNA (gDNA) from seedlings at the two to three leaf stage.

Microsatellite markers and PCR amplification

Eleven wheat microsatellite markers for 11 loci located in the chromosomes 1A, 2A, 2D, 3A, 3B, 4D, 5D, 6B and 7D, were used for genetic diversity analysis. Xgwm and Xwmc markers were obtained, respectively from Röder et al. (1998) and Somers and Isaac (2004; Grain Genes).

PCR reactions were carried out in 14 µl reaction mixtures of KAPA2GTM Fast Multiplex PCR Mix, 6.25 µM of each forward and

*Corresponding author: E-mail: wcb@sun.ac.za.

Table 1. Wheat cultivars used and their origins in Cameroon.

S/N	Samples' names	Local name	Village	Region
1	Ngm 2	Ngm 2	Wassande	Adamawa
2	Fuanb2	Fuanb2	Fuanentui	Northwest
3	Babankit	Babankit	Smal Babanki	Northwest
4	Alexander wonder	Alexander wonder	Boyo	Northwest
5	Fuanb1	Fuanb1	Fuanentui	Northwest
6	Sonalika	Sonalika	Wassande	Adamawa
7	Fuanb3	-	Fuanentui	Northwest
8	Fuanb4	-	Fuanentui	Northwest
9	HGW	Hard wheat	Abongphen	Northwest
10	BBT2		Abongphen	Northwest
11	WASSANDE 2	WASSANDE 2	Wassande	Adamawa
12	Vrack	Vrack	Bambui	Northwest
13	Ngderem4	-	Wassande	Adamawa
14	Ngderem1	Ngderem1	Wassande	Adamawa
15	Ngderem3	-	Wassande	Adamawa
16	IRAT 10	IRAT 10	Bambui	Northwest
17	RIBA	RIBA	Boyo	Northwest

reverse primer, 1 µl gDNA and dH_2O. The PCR cycling conditions was set at 94°C for 3 min of denaturation, followed by 45 cycles of 1 min at 94°C, 1 min at the annealing temperature (Ta), 2 min at 72°C and then 72°C for 10 min for extension.

The PCR products were electrophoresed on 6% non-denaturing polyacrylamide gels containing 1xTBE (Tris Borate EDTA). The amplified band sizes for each SSR locus were determined on the basis of their migration relative to the 50 bp marker.

Data analysis

The molecular diversity within all accessions was estimated for each SSR locus, using the Power Marker 3.25 software (Liu and Muse, 2005). To measure the informative character of the SSR markers, the PIC for each marker was calculated using the formula of Nei (1973):

$$PIC = 1-\Sigma_{i=1}^{k} P_i^2$$

Where, k is the total number of alleles detected per locus and Pi the frequency of the allele i in all 17 accessions.

Genetic similarity (GS; Dice, 1945) was calculated as:

$$GS = 2N_{ij}/(N_i + N_j)$$

Where, N_{ij} is the number of fragment common to individual i and j, and (Ni + Nj) is the total number of fragment in both individuals.

Genetic distance (GD) among group pairs was calculated following Nei and Li (1979),

$$(GD_{xy}) = 1-(2N_{xy}/N_x + N_y)$$

The dendrogram was constructed using the method based on the genetic distance (SAHN method, UPGMA algorithm) of the 17 accessions and using the software Statistica 12. To calculate allele frequency (A_{xy}) from one of the variation to another in each locus, the formula of Khlestkina et al. (2004) was used:

$$A_{xy} = \Sigma|P_{xi} - P_{yi}|N_{xy}$$

Where, P_{xi} and P_{yi} are the frequencies of the i^{th} allele in regions X and Y, respectively, and N_{xy} is the total number of alleles for the two groups X and Y. The allelic frequency variation was calculated separately for each of the 11 loci and then for all of them as an average. All fragments were used to generate GS matrix for Principal Component Analysis (Sneath and Sokal, 1973).

RESULTS

Characteristics of markers and genetic diversity

All pairs of primers specific for SSR locus used resulted in a positive amplification with allelic variations in size on all DNA of wheat accessions. A total of 77 microsatellite alleles were detected. The number of alleles per locus varied from 2 (Xgwm 125 and Xgwm 331) to 13 (Xwmc 177), with an average of 7 alleles per locus. Genetic diversity for microsatellite loci ranged from 0.46 (Xgdm 125) to 0.90 (Xgwm 177) with an average of 0.88. The polymorphism information Content (PIC) varied from 0.25 (Xwmc 331) to 0.89 (Xwmc 177), with an average of 0.69 (Table 2).

The results indicated a significant correlation ($P < 0.01$) between gene diversity and number of alleles across wheat accessions in both Regions (Figure 1). The correlation coefficient between these two variables over the 11 loci were 0.88 (Adamawa) and 0.76 (Northwest).

Genetic relationship and diversity among different geographical regions

Genetic distance value (GD) indicates that some

Table 2. Description of SSR Markers.

Locus	Chromosome position	Primers sequences	Repeat	Bases expected	Annual temperature	Alleles frequency	Number of alleles	Gene diversity	PIC
Xwmc 11	1A, 3A	5' TTGTGATCCTGGTTGTGTTGTGA 3' 5' CACCCAGCCGTTATATATGTTGA 3'	CT	177	61	0.29	8	0.83	0.81
Xwmc 59	1A. 6A	5' TCATTCGTTGCAGATACACCAC 3' 5' TCAATGCCCTTGTTTCTGACCT 3'	(CA)19	197	58	0.18	10	0.89	0.87
Xwmc 177	2A	5' AGGGCTCTCTTTAATTCTTGCT 3' 5' GGTCTATCGTAATCCACCTGTA 3'	(CA)21	184	52	0.18	13	0.90	0.89
Xgwm 190	5D	5' GTGCTTGCTGAGCTATGAGTC 3' 5' GTGCCACGTGGTACCTTTG 3'	(CT)22	201-253	55	0.18	9	0.87	0.86
Xgwm 437	7D	5' GATCAAGACTTTTGTATCTCTC 3' 5' GATGTCCAACAGTTAGCTTA 3'	(CT)24	109-111	47	0.18	10	0.88	0.87
Xgwm 539	2D	5' CTGCTCTAAGATTCATGCAACC 3' 5' GAGGCTTGTGCCCTCTGTAG 3'	(GA)27	143-157	60	0.24	8	0.83	0.81
Xdgm 125	4D	5' GCAGGCGTGTTACTCCAAGT 3' 5' CCGAGGTGGATAGGAGGAAA 3'	-	-	60	0.65	2	0.46	0.35
Xwmc 331	4D	5' CCTGTTGCATACTTGACCTTTTT 3' 5' GGAGTTCAATCTTTCATCACCAT 3'	-	128	61	0.82	2	0.29	0.25
Barc 133	3B	5' AGCGCTCGAAAAGTCAG 3' 5' GGCAGGTCCAACTCCAG 3'	(CT)24	-	-	0.65	4	0.52	0.47
Xgwm 133	6B	5' ATCTAAACAAGACGGCGGTG 3' 5' ATCTGTGACAACCGGTGAGA 3'	(CT)39	-	-	0.35	4	0.72	0.67
Xgwm 644	6B	5' GTGGGTCAAGGCCAAGG 3' 5' AGGAGTAGCGTGAGGGGC 3'	(GA)20	-	-	0.29	7	0.79	0.76
Mean	-	-	-	-	-	0.36	7	0.72	0.69

Xgwm and Xwmc markers were obtained respectively from Röder et al. (1998) and Somers and Isaac (2004; Grain Genes); PIC, Polymorphism information content.

accessions are closely related. The GD over accessions in all regions ranged from 0.18 (between Wassande2 and NGDEREM3) to 1 with a mean of 0.8 (80%). So, at 80% of genetic divergence, the 17 wheat cultivars studied were structured into 5 main groups (A, B, C, D and E) in the dendrogram based on the UPGMA analysis using SSR data (Figure 2). Group A included 4 cultivars (Alexander wonder, Riba, Vrack and FUANB3).

Very close to 80% of genetic dissimilarity, the group B could be divided into two subgroups: subgroup B1 contained 6 accessions (BABANKIT, FUANB1, FUANB4, FUANB2, BBT2 and HGW) while subgroup B2 included only one cultivar (IRAT 10). It is noteworthy that the two varieties FUANB1 and FUANB4 are identical. Group C contained 4 cultivars (Ngderem1, Ngderem3, WASSANDE 2 and NGM2) while Groups D and E each contained 1 cultivar, respectively (Ngderem4 and SONALIKA).

Furthermore, the principal component analysis (PCA) for the six-collection village split the accessions into five clearly distinct groups. The first two principal components had Eigen values of 6.36 and 3.81. The PCA grouped the 17 wheat accessions into various components with the first two explaining 59.86 and 37.44% of the total variation. Accessions from each village were approximal clustered together (Figure 3). So, 80% of the genetic material from the same geographical village could be clustered in specific groups.

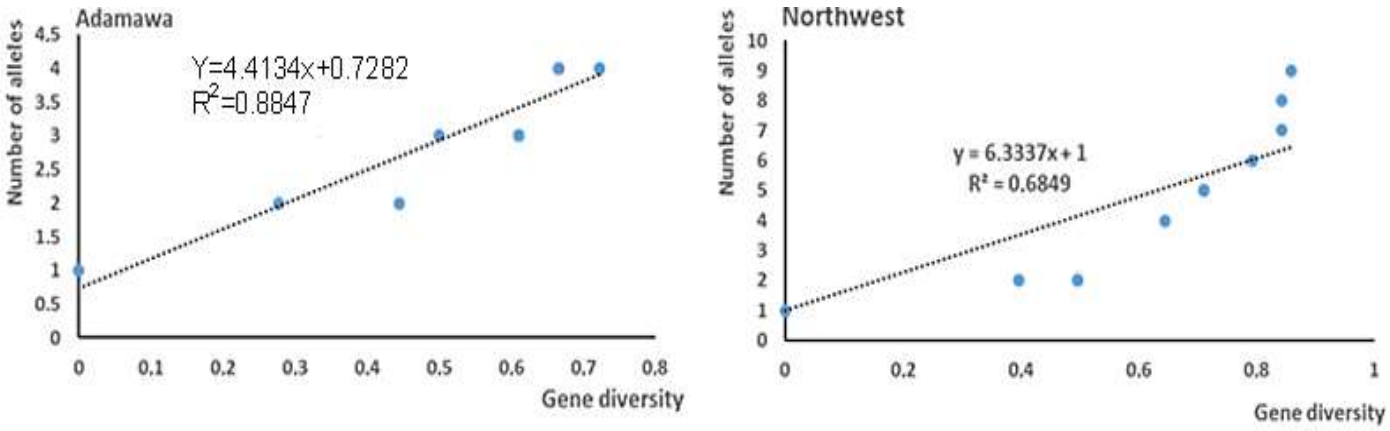

Figure 1. Correlation between gene diversity and the number of alleles over 11 microsatellite loci in hexaploid wheat.

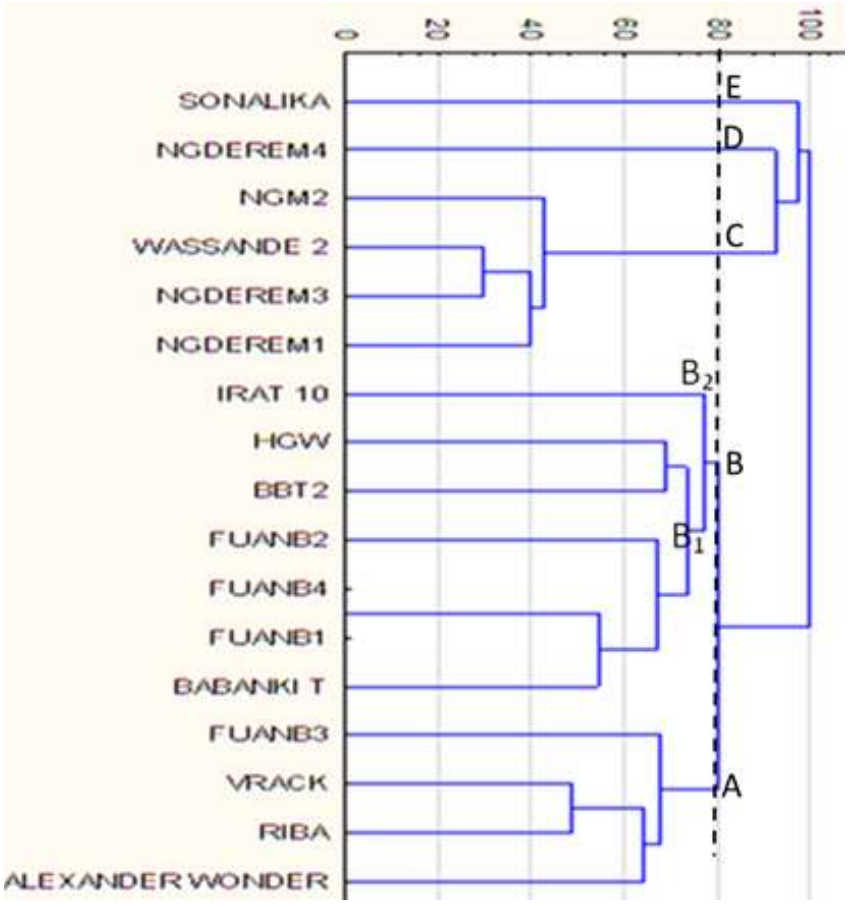

Figure 2. Grouping according to the dissimilarities between 17 accessions of hexaploid wheat on the basis of the SSR profiles of 11 loci.

Accessions were then analyzed separately according to their region of origin (Adamawa and Northwest). A comparison of the genetic diversity of wheat accessions was done between two germplasm pools. The mean of gene diversity, number of alleles per locus, total number of alleles and the number of accessions carrying rare alleles were higher in Northwest, compared to those in Adamawa Region (Table 3). These results suggest that

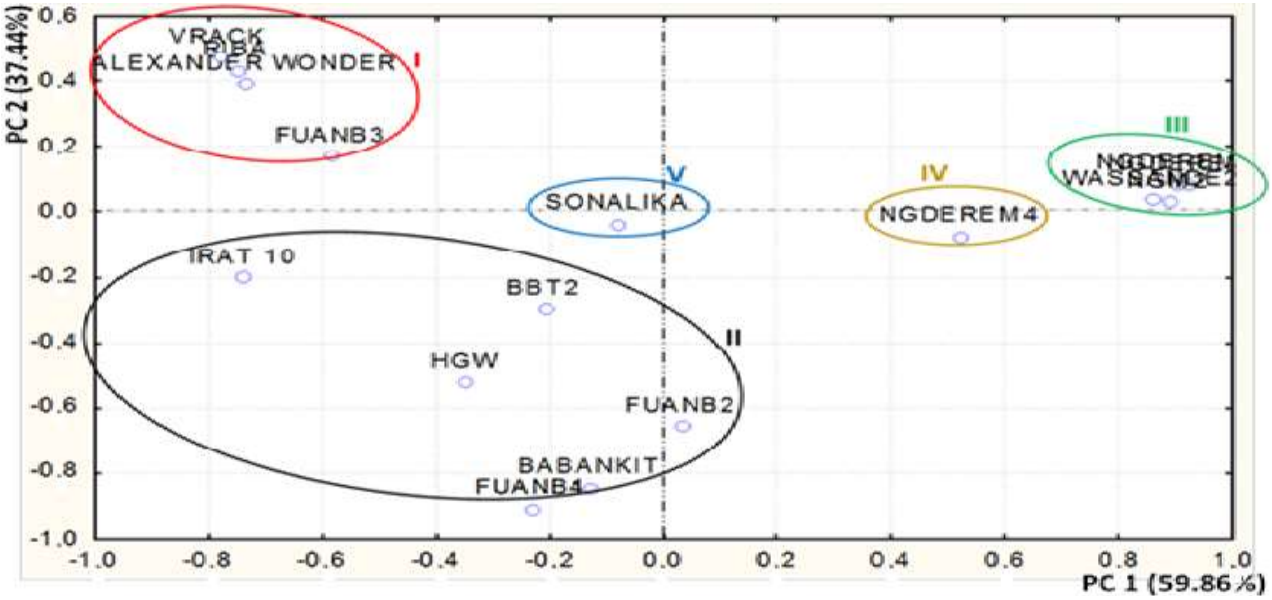

Figure 3. Principal component analysis of 17 hexaploid wheat accessions from 6 villages in Cameroon. The grouping is based on Dice's similarity coefficients.

Table 3. Analysis of geographical regions.

Item	Northwest	Adamawa
Number of accessions	n = 11	n= 6
Total number of alleles	51	34
Average number of alleles per marker	4.64	3.09
Number of rare alleles	5	6
Mean of PIC-values	0.57	0.48
Mean of Gene diversity	0.62	0.54

the Northwest area exhibited greater genetic diversity than Adamawa region, even after taking into account the effect of collection size.

DISCUSSION

Diversity of SSR markers

In the present study, 11 microsatellite markers revealing 77 alleles allowed to discriminate 17 cultivars of hexaploid wheat collected in Cameroon. The number of alleles per locus ranged from 2 to 13 with an average of 7. Röder et al. (2002) detected an average of 10.5 alleles per locus from 502 recent European wheat varieties, using 19 microsatellite markers. Khaled et al. (2015) used 17 SSR markers to assess genetic diversity of 33 genotypes of hexaploid wheat from Egypt and detected an average of 5.59 alleles per locus.

The average number of alleles per locus in the study is thus comparable to those observed in previous studies. In addition, the microsatellite markers we used had an average PIC value of 0.69, which means that these markers are highly informative in our study. Indeed, Botstein et al. (1980) reported that a PIC value higher than 0.5 is considered to be a sign of a very informative marker, while 0.5> PIC> 0.25 corresponding to an informative marker. In previous studies, Röder et al. (2002) found an average PIC value of 0.67 in 500 genotypes. The choice of these SSR loci is therefore relevant for our study.

Genetic relationship between wheat cultivars

Cluster analysis discriminated all cultivars of Cameroonian hexaploid wheat into five main groups. Most cultivars clustered according to their geographical location. Indeed, all accessions from groups B and C are cultivated in the Northwest and Adamawa Regions,

respectively. Similarly, the 4 varieties of group A were collected in the Northwest Region. Moreover, the variety NGDEREM4 of group D comes from Adamawa and the SONALIKA variety of group E was introduced in Cameroon since 1975 through the SODEBLE Company, from Mexico. Huang et al. (2002) reported that the genetic diversity of hexaploid wheat was not completely related to geographic distribution. They also reported that, these results might be explained by the fact that similar genetic variation occurred independently in the different geographic regions or that artificial transfer of accessions from one region to others resulted in a false determination of the geographic origin.

Similar results were obtained by Khaled et al. (2015) in hexaploid wheat genotypes grown in Egypt. On the other hand, Al-Khanjari et al. (2007) found that all local varieties of wheat from the same geographical area clustered in the same group. In our case, we can hypothesize that the genetic proximity of the cultivars based on their geographical origin results from a local selection and diversification, coupled with weak or non-existent exchanges of seeds between regions, inducing a geographical structuration and a form of isolation by distance.

The overall gene diversity increased with the number of alleles at a given locus. We found significant correlation between gene diversity and the number of alleles in Adamawa ($r = 0.88$, $P < 0.01$) and Northwest ($r = 0.76$, $P < 0.01$). Therefore, the number of alleles could be used for the assessment of genetic diversity in hexaploid wheat. Similar results were found by Huang et al. (2002) in a set of 24 microsatellite markers used to characterize 998 accessions of hexaploid wheat germplasm. Consequently, these authors reported that the characterization of a reliable correlation coefficient needs a large sample size. The results in the present study disagrees with those reported by Prasad et al. (2000) who indicated that the polymorphism information content value was not correlated with the number of alleles in 55 wheat accessions. According to Huang et al. (2002), the number of alleles was also correlated with the repeat number of microsatellite DNA and its relative distance from the centromere. It has been suggested that the three mechanisms for creating a new allele at SSR loci are slippage replication (Tachida and Iizuka, 1992), unequal crossing-over and genetic recombination (Harding et al., 1992). The value of genetic distance (GD) indicated that some accessions were closely related. Averages of GD over accessions in all regions were ranged from 0.18 (between Wassande2 and NGDEREM3) to 1 with a mean of 0.8 (80%). The high GD coefficient values indicate the presence of high gene diversity in the accessions.

The mean of gene diversity was relatively higher in Northwest (0.62) compared to Adamawa (0.54). These results suggested that the Northwest exhibited greater genetic diversity than Adamawa region. The Northwest was the presumed center of origin of hexaploid wheat in Cameroon and Adamawa was the sites were the SODEBLE was established. The results obtained in our study provided new information on the relationships between the Cameroonian bread wheat cultivars.

The set of the used microsatellite markers showed a high level of polymorphism and sufficient information to discriminate the cultivars of hexaploid wheat grown in Cameroon. Generally, our study provides a first description about the molecular genetic diversity of Cameroonian wheat varieties. The results are consistent with expectations and provide a first base for further investigations. The important level of the genetic diversity reported in the present study should be taken into account in developing wheat breeding programs in agro-ecological zones of Cameroon. Morphological and phenotypic studies will also be required to couple our results of molecular analyzes.

CONFLICT OF INTERESTS

The authors have not declared any conflict of interests.

ACKNOWLEDGMENTS

This collaborative work was supported by the « MIC-CERES » project (Microbial eco-compatible strategies for improving wheat quality traits and rhizospheric soil sustainability) jointly supported by Agropolis Fondation (grant AF Project ID 1301-003) through the "Investissements d'avenir" programme (with reference number ANR-10-LABX-0001-01) and Fondazione Cariplo (grant FC Project ID 2013-1888), and European Commission through PAFROID projects (*INTRA-ACP Program, lot Africa for an action N°2013- 4644 / 001 – 001 with the reference: 384201-EM-1-2013-1-MG-INTRA_ACP*). The authors are grateful to the Plant Breeding Laboratory staff of Stellenbosch University for their technical support during the molecular analyses in laboratory. They would like to thank Dr. Apollinaire Tagne, Yves H. Tchiechoua, Adrienne N. Ngom, Aga Valentine Enwe and Tume George Tardzenyuy for their technical assistance during the samples collection.

REFERENCES

Akfirat FS, Uncuoglu AA (2013). Genetic diversity of winter wheat (*Triticum aestivum* L.) revealed by SSR markers. Biochem. Genet. 51:223-229.

Al-Khanjari S, Hammer K, Buerkert A, Röder MS (2007). Molecular diversity of Omani wheat revealed by microsatellites: II. Hexaploid landraces. Genet. Resour. Crop Evol. 54:1407-1417.

Allen AM, Winfield MO, Burridge AJ, Downie RC, Benbow HR, Barker GL, Wilkinson PA, Coghill J, Waterfall C, Davassi A, Scopes G (2017). Characterization of a Wheat Breeders' Array suitable for high-throughput SNP genotyping of global accessions of hexaploid bread wheat (*Triticum aestivum*). Plant Biotechnol. J. 15(3):390-401.

Ayuk-Takem J (1984). Performance de 12 variétés de blé (*Triticum aestivum* L.) en croissance à UPPER FARM (1982 m). Rapport d'activités annuelles de IRA (Institut de la Recherche Agronomique) Bambui, pp.1982-1986.

Bohn M, Utz HF, Melchinger AE (1999). Genetic similarities among winter wheat cultivars determined on the basis of RFLPs, AFLPs and SSRs and their use for predicting progeny variance. Crop Sci. 39:228-237.

Botstein D, White RL, Skolnick M, Davis RW (1980). Construction of a genetic linkage map in man using restriction fragment length polymorphisms. Am. J. Hum. Genet. 32:314-331.

Dice LR (1945). Measures of the amount of ecologic association between species. Ecology 26:297-302.

Doyle JD, JL Doyle (1990). Isolation of plant DNA from fresh tissue. BRL Focus 12:13-15.

Froese PS, Carter AH (2016). Single Nucleotide Polymorphisms in the Wheat Genome Associated with tolerance of Acidic Soils and Aluminum Toxicity. Crop Sci. 56:1662-1677.

Fu YB, Peterson GW, Richards KW, Somers D, DePauw RM, Clarke JM (2005). Allelic reduction and genetic shift in the Canadian hard red spring wheat germplasm released from 1845 to 2004. Theor. Appl. Genet. 110:1505-1516.

Gorji AH, Zolnoori M (2011). Genetic diversity in Hexaploid Wheat Genotypes using Microsatellite Markers. Asian J. Biotechnol. 3(4):368-377.

Grassini P, Eskridge KM, Cassman KG (2013). Distinguishing between yield advances and yield plateaus in historical crop production trends. Nat. Commun. 4:2918-000.

Harding RM, Boyce AJ, Clegg JB (1992). The evolution of tandemly repetitive DNA: recombination rules. Genetics 132:847-859.

Huang XQ, Börner A, Röder MS, Ganal MW (2002). Assessing genetic diversity of wheat (*Triticum aestivum* L.) germplasm using microsatellite markers. Theor. Appl. Genet. 105:699-707.

Khaled FMS, Röder MS, Börner A (2015). Assessing genetic diversity of Egyptian hexaploid wheat (*Triticum aestivum* L.) using microsatellite markers. Genet. Resour. Crop Evol. 62:377-385.

Khlestkina EK, Röder MS, Efremova TT, Börner A, Shumny VK (2004). The genetic diversity of old and modern Siberian varieties of common spring wheat as determined by microsatellite markers. Plant Breed. 123:122-127.

Liu K, Muse SV (2005). PowerMarker: Integrated analysis environment for genetic marker data. Bioinformatics 21(9):2128-2129.

Mukhtar MS, Rehman M, Zafar Y (2002). Assessment of genetic diversity among wheat (*Triticum aestivum* L.) cultivars from a range of localities across Pakistan using random amplified polymorphic DNA (RAPD) analysis. Euphytica 28:417-425.

Nei M (1973). Analysis of gene diversity in subdivided populations. Proc. Natl. Acad. Sci. USA 70:3321-3323.

Nei M, Li WH (1979). Mathematical model for studying genetic variation in terms of endonucleases. Proc. Natl. Acad. Sci. USA 76:5269-5273.

Prasad M, Varshney RK, Roy JK, Balyan HS, Gupta PK (2000). The use of microsatellites for detecting DNA polymorphism, genotype identification and genetic diversity in wheat. Theor. Appl. Genet. 100:584-592.

Rajaram S, Hettel GP (1994). Wheat Breeding at CIMMYT: Wheat special report N° 29. Ciudad Obregon, Sonora, Mexico 21-25 March, 1994.

Reza MD, Goodarz N, Elham Aram S (2015). Investigation of genetic diversity of some durum and bread wheat genotypes using SSR markers. J. Biodivers. Environ. Sci. 6(3):24-32.

Röder MS, Korzun V, Wendehake K, Plaschke J, Tixier MH, Leroy P, Ganal MW (1998). A microsatellite map of wheat. Genetics 149:2007-2023.

Röder MS, Wendehake K, Korzun V, Bredemeijer G, Laborie D, Bertrand L, Isaac P, Rendell S, Jackson J, Cooke RJ, Vosman B, Ganal MW (2002). Construction and analysis of a microsatellite-based database of European wheat varieties. Theor. Appl. Genet. 106:67-73.

Ryan PR, Raman H, Gupta S, Horst WJ, Delhaize E (2009). A second mechanism for aluminum resistance in wheat relies on the constitutive efflux of citrate from roots. Plant Physiol. 149 340-351.

Sneath PHA, Sokal RR (1973). Numerical Taxonomy. Freeman. San Francisco. P. 573.

Somers DJ, Isaac P (2004). SSRs from the Wheat Microsatellite Consortium. Available at< wheat. pw. usda. gov/ggpages/SSR/WMC> Accessed on March 10 (2004): 2010.

Sonmezoglu OA, Bozmaz B, Yildirim A, Kandemir N, Aydin N (2012). Genetic characterization of Turkish bread wheat landraces based on microsatellite markers and morphological characters. Turk. J. Biol. 36:589-597.

Tachida W, Iizuka M (1992). Persistence of repeated sequences that evolve by replication slippage. Genetics 131:471-478.

academicJournals

Vol. 16(36), pp. 1840-1848, 6 September, 2017
DOI: 10.5897/AJB2017.16070
Article Number: ADD838A65905
ISSN 1684-5315

http://www.academicjournals.org/AJB

African Journal of Biotechnology

Full Length Research Paper

Expression and functional evaluation of *Mytilus galloprovincialis* foot protein type 5 (Mgfp-5), the recombinant mussel adhesive protein

Yawei Lv, Yujing Zhang, Wenying Gao and Yingjuan Wang*

Key Laboratory of Biotechnology, China College of Life Science, Northwest University, Shaanxi, 710069, Xi'an, China.

Received 14 May, 2017; Accepted 24 August, 2017

Mussel contains a variety of adhesion proteins, among which, *Mytilus galloprovincialis* foot protein type 5 (Mgfp-5) is one of the major proteins required for substrate adhesion. The labor-intensive nature and insufficiency of the extraction process have frequently resulted in very little purified recombinant Mgfp-5. These prompt technologies such as chemical synthesis and genetic engineering are employed to overcome these limitations. In this study, successful expression and purification of the recombinant Mgfp-5 using *Escherichia coli* BL21 (DE3) and affinity chromatography were reported. Production yield of 12.25% and purity of 96.92%, respectively were observed. The 3,4-dihydroxyphenylalanine (DOPA) content (9.60 pmol/g) and the adhesion (1 116 nN) in modified recombinant Mgfp-5 were 9.32 times and 1.6 times as great as those in the unmodified recombinant Mgfp-5, respectively. Recombinant Mgfp-5 at a concentration of 9.6 mg/L had little cytotoxicity on mouse L-929 fibroblast cells, which was toxic at first in cytotoxicity test, and a concentration of not more than 20 µg/mL would not lead to hemolysis of rabbit erythrocytes. In this case, recombinant Mgfp-5 is biosecure, providing the foundation for Mgfp-5 manufacturing as well as the development of clinical biological adhesive.

Key words: Mgfp-5, 3,4-dihydroxyphenylalanine (DOPA), adhesion, cytotoxicity, hemolysis.

INTRODUCTION

Marine mussel secretes a specific adhesive protein by its byssus to survive an aqueous environment. This was first observed in the 1980s by researchers and is called *Mytilus* adhesive protein (MAPs) or *Mytilus* foot protein (Mfps) (Waite and Tanzer, 1981). MAPs are one of the potential resources in the field of biotechnological applications for its strong adhesion, flexibility, water resistance and biodegradability, among others (Dove and Sheridan, 1986). MAPs can strongly adhere to surface of various materials under wet conditions, such as glass, plastic, metal, wood, and even polytetrafluoroethylene. Moreover, they can effectively bind to biological tissues or organs, and as a result, are applied in dentistry, dermatology, orthopedics and ophthalmology without noticeable toxicity and immunogenicity (Wu et al., 2014; Waite, 2002).

*Corresponding author. E-mail: wangyj@nwu.edu.cn. Tel: +86 18629326118.

Mussel byssus can be divided into proximal thread and distal plate, which secretes 6 types of proteins (Mfp-1 to Mfp-6) and three kinds of precollagens (preCol), namely, preCol-D, preCol-P and preCol-NG MAPs (Rego et al., 2016). These MAPs are rich in unusual amino acid 3,4-dihydroxyphenylalanine (DOPA) that can be catalyzed by polyphenol oxidase, which is central to the cross-linking reactions of cohesive curing and adhesive surface bonding (Silverman and Roberto, 2007). It has been proved that DOPA content is correlated with the adhesive strength of MAPs (Yu et al., 1999). Mfp-5 is located in the byssus plate where the DOPA content is approximately 30% (Waite, 2011). Hence, it directly plays a major role in adhesion (Waite, 2011).

Becton, Dickinson (BD Bioscience) companies have extracted the Mfp-1 and Mfp-2 mixtures (Cell-Tak^{TM}) which have been applied in biological adhesive products using the natural method. However, only one (1) mg of the protein can be obtained from about 10 000 mussels by natural extraction. Inefficiency and high cost of such natural extraction process has greatly restricted the application of MAPs. On this basis, chemical synthesis and genetic engineering have been widely applied, attempting to solve the above-mentioned difficulties (Gim et al., 2008; Platko et al., 2008). In this study, the recombinant *Mytilus galloprovincialis* foot protein type 5(Mgfp-5) was successfully expressed in *Escherichia coli* BL21 (DE3) and purified, and the cytotoxicity of protein should be further tested in order to examine whether the recombinant Mgfp-5 could reach the safety standard or not.

The current study focused on the issue of, how recombinant Mgfp-5 could be expressed in *E. coli* and purified by nickel (Ni^{2+}) column affinity chromatography. Subsequently, biological adhesion of recombinant Mgfp-5 was measured by glass coating and atomic force microscopy (AFM). Meanwhile, biological safety was analyzed by cell cytotoxicity test (Cell Counting Kit and CCK 8 qiagen method) and hemolysis test, in order to lay a good foundation for the development and application of sources of biological adhesive.

MATERIALS AND METHODS

Expression of recombinant Mgfp-5 protein

The pUC57 containing the Mgfp-5 gene (constructed and preserved in our laboratory) was constructed according to the sequence of cDNA Mgfp-5 (Gen Bank: AY521220. 1) gene. The plasmid pET28a-mgfp was constructed for Mgfp-5 gene and pET-28a vector using the following primers: F (*Nde* I cleavage site and protecting bases): 5'-GGAATTCCATATGAGTTCTGAAGAAT, and R (*EcoR* I cleavage site protecting bases): 5'-CGGAATTCCTAACTGCTACCACCT. PCR amplification program: 94°C pre-denaturation 5 min; 94°C denaturation 30 s; 55°C annealing 30 s; 72°C extension 45 s, cycle 34 times, 72°C extension 10 min were used. The purified amplified product and pET-28a vector were digested with *Nde* I and *EcoR* I, respectively, which were ligated with T4-DNA ligase and then transformed into *E. coli* BL21 on LB plates containing 50 mg/L Kan at 37°C overnight culture.

Monoclonal *E. coli* BL21 lacking the Mgfp-5 gene and *E. coli* BL21-Mgfp with the Mgfp-5 gene were cultured overnight in Luria Broth (LB, contained 50 Kan) followed by centrifugation at 200 r/min and 37°C, respectively. Plasmid pET28a-mgfp was extracted from *E. coli* strains, and PCR DNA products were separated on 0.8% (w/v) agarose gel.

Bacteria were propagated and cultured at a proportion of 1:100. Subsequently, bacterial cultures were induced by isopropyl β-D-thiogalactoside (IPTG, 1.0 mmol/L) at OD_{600} = 0.8. 4 h later, 1.0 mL bacteria liquid was centrifuged at 4°C and 12 000 r/min for 10 min, and cells were collected. Expression of recombinant Mgfp-5 was analyzed by 15% sodium dodecyl sulfate polyacrylamide gel electrophoresis (SDS-PAGE).

Purification of recombinant Mgfp-5 protein

E. coli BL21-Mgfp were cultured using batch bioreactor (Sartorius). Subsequently, recombinant Mgfp-5 was purified using Ni^{2+} affinity purification under natural or denaturing conditions, containing 8 mol/L urea as previously described (Lv et al., 2016). Following this, western blotting using His_6 tag was carried out.

The content of the protein was measured using a BCA Protein Assay Kit-Reducing Agent Compatible (Thermo Fisher Scientific, China) according to the manufacturer's instructions, with bovine serum albumin as the standard. The purity from the purified protein was evaluated by gradation analysis, while the pure protein was freeze-dried and stored at -80°C.

Modification of proteins

Purified protein was dissolved in phosphate buffered saline (PBS) (NaCl 0.1 mmol/L, KCl 3 mmol/L, $Na_2HPO_4{\cdot}12H_2O$ 10 mmol/L, KH_2PO_4 2 mmol/L) containing 10 mmol/L ascorbic acid and 20 mmol/L sodium borate (0.1 mol, pH 7). In order to modify tyrosine residues to DOPA, the solution was irregularly oscillated for 2 h at room temperature after adding 10 U/mL tyrosinase. Recombinant Mgfp-5 was collected by ultrafiltration and dialysis in 5% acetic acid. Bovine serum albumin (BSA) was used as the negative control and Cell-Tak^{TM} as the positive control.

DOPA content analysis

DOPA content was measured by nitroblue tetrazolium and potassium glycinate (NBT/glycinate, 0.24 mmol/L NBT in 2 mo/L potassium glycinate, pH 10) staining assay. The DOPA standard (1 μg/mL) was dispensed (0, 2, 4, 8, 16 and 20 μL) and added into six labeled wells in a 96-cell well format. The final volume of each well was adjusted to 20 μL with Milli-Q water and NBT/Glycinate (180 μL) was added.

All reagents were pipetted into tubes immersed in an ice-water bath. This reaction started by incubating in water bath at 25°C in the dark. An hour later, optical density (OD) was measured at a wave length of 530 nm. DOPA quantity of samples was determined from the standard curve and Milli-Q water was used as a negative control.

Adhesion analysis

Protein samples (10 μL of 1.00 mg/mL) were added into the glass surface and incubated under a humid environment at 25°C for 12 h. The surfaces were dried using natural drying and each was washed thoroughly with Milli-Q water for 2 h with shaking. Protein coating

spots were visualized using Coomassie brilliant blue staining. Images of protein spots were captured using a scanner and were analyzed by PDQUest software according to the protocols provided by Bio-Rad. BSA was used as a negative control.

AFM cantilevers were modified in accordance with techniques adopted by Ducker et al. (1991). The spring constant of AFM (SPM-9500J3) was 5 N/m. A lass sphere (Duke Scientific) of 5 μm in diameter was attached to the tip of cantilever using an epoxy resin (Vantico) under microscope, and the modified cantilever was cured at room temperature for 24 h. The modified AFM cantilevers were mounted onto cells and allowed to contact with 2 μL sample solutions (1.0 mg/mL) on glass slides for 20 min; this allow proteins to adsorbed on the glass bead.

After 10 min of contact, a force-distance curve was obtained by separating the modified cantilever from the glass surface. The pulling velocity for the force-distance curve was measured as 1 mm/s. Recombinant Mgfp-5 was dissolved in PBS and the final concentration was 1 mg/mL, which adhered to spearhead (polytetrafluoroethylene) and centrifugal tube cover (propathene) with different sizes or weights. Macroscopic adhesion conditions of protein were observed.

Cytotoxicity test

According to the rule of MAP wound dressing in the use of the human body (usage amount of the 2% human body area less than 1 mL per day), the amount of MAP was 3.0 μg/cm^2 (Liu et al., 2013). In this study, the mass concentration of Mgfp-5 should be 9.6 mg/L on the base of 96 well culture plate (Per well area is 0.32 cm^2 and medium is 0.1 mL in per well). L-929 cells cultured in the Dulbecco's modification of Eagle's medium Dulbecco (DMEM) supplemented with 10% fetal bovine serum (100 μL) were added to the 96-well cell plate and cultured to cell adherence in a CO_2 incubator at 37°C.

After replacing fresh broth, protein samples (100 μL of 9.6 mg/L) were added in every well. Cell morphology was evaluated 2 days later using inverted phase contrast microscope. Subsequently, CCK-8 (Rainbio) (10 μL) was added into each well and the absorbance value (A) was recorded at 450 nm after 4 h. Relative growth rate (RGR) was calculated using:

$$\mathrm{RGR}\ (\%) = \frac{\text{average absorbance value}}{\text{average absorbance value of bank control}} \text{x } 100\%$$

Cytotoxicity of recombinant Mgfp-5 was evaluated according to ANSI/AAMI/ISO 10993-5:1999 (Table 1). In addition to the blank (cell culture medium DMEM), a negative (PBS) and positive control (9.6 mg/L dimethyl sulfoxide, DMSO) was included in the experiment. All assays were repeated for at least three times to ensure the reproducibility.

Hemolytic test

On entering of Mgfp-5 into the body, hemolysis is one of the most important concerns regarding its safety. In the present study, 2% of the rabbit red blood cell (RBC) suspension was obtained by centrifugation and suction to remove the serum from the blood and further washed five times with sterile normal saline solution. Cells were diluted to 2/100 in a volume with normal saline solution.

2 mL of the diluted RBC suspension was mixed with 2 mL recombinant Mgfp-5 solution at different concentrations, ranging from 5, 10, 20 to 25 μg/mL and incubated immediately at 37°C. Incubation of all was sequentially performed for 0.5, 1, 2 and 3 h, followed by centrifugation at 1 000 rpm for 15 min. The hemolysis of RBC was observed and the hemolysis ratio was evaluated. In A value, the supernatant solution was recorded by spectrophotometer at 545 nm wave length. 0.9% sterile sodium chloride solution and sterile water were used as the negative and positive controls, respectively. In ANSI/AAMI/ISO 10993-4:2002/A1:2006 standard, the test sample was considered as hemolytic if the rate of hemolysis was >5%. Finally, the hemolytic ratio was expressed as percentage and was calculated as follows:

$$\text{Hemolysis ratio}\ (\%) = \frac{\mathrm{A_{sample}} - \mathrm{A_{negative}}}{\mathrm{A_{positiven}} - \mathrm{A_{negative}}} \text{x } 100\%$$

All assays were repeated at least three times to ensure the reproducibility.

Table 1. Reactivity grades of cytotoxicity.

RGR (%)	Cytotoxicity grade	Instructions
≧100.0	0	Non-toxic
75-99	1	Very mild toxicity
50-74	2	Mild toxicity
25-49	3	Moderate toxicity
1-24	4	Severe toxicity
0	5	Heavy toxicity

RESULTS

Expression of recombinant Mgfp-5 protein

The PCR assay results are indicated in Figure 1A; these showed amplification of the specific 260-bp band of Mgfp-5 gene fused with hexahistidine affinity ligand, which is clearly absent with the negative control. Recombinant Mgfp-5 was successfully expressed with the apparent molecular weight on SDS-PAGE gel, being greater (about 15 KD) than the predicted one (about 11.4 KD) (Figure 1B) which might be attributed to the higher isoelectric point (9.8) of recombinant Mgfp-5 as well as the combination with SDS (Hwang et al., 2010).

Purification and modification of proteins

Recombinant Mgfp-5 under natural or denaturing conditions (containing 8 mol/L urea) was analyzed. SDS-PAGE analysis indicated that recombinant Mgfp-5 was successfully expressed using IPTG induction and was purified by Ni^{2+} column chromatography (Figure 1C). In addition, yield of dissociated recombinant Mgfp-5 under denaturing condition was much higher than that under natural conditions.

Recombinant Mgfp-5 (37.00±2.55 mg) was purified from 1 L denaturing lysis buffer containing 302.00±16.55 mg of total protein, with the efficiency of about 12.25% and the purity reaching 96.92%. The analysis also showed that some recombinant Mgfp-5 exist as a dimer.

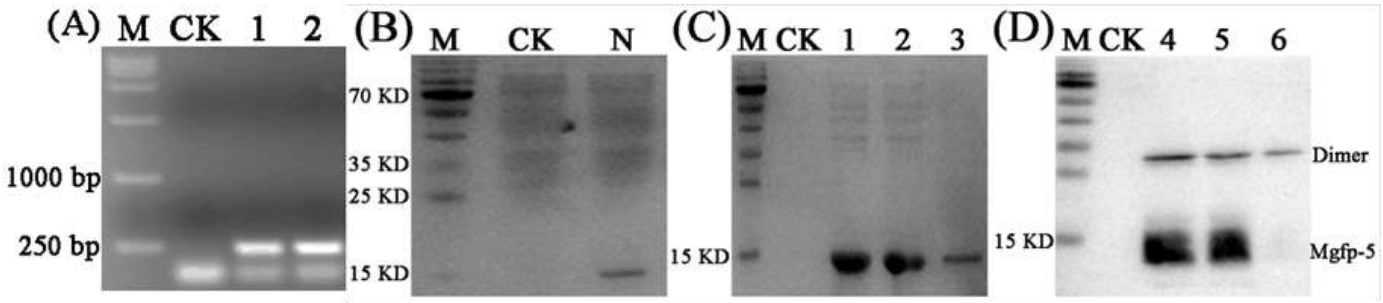

Figure 1. Expression and purification of recombinant Mgfp-5 from *E. coli* BL21. PCR analysis of plasmid from *E. coli* BL21 and *E. coli* BL21-mgfp (A). Lanes: M, DNA Marker; CK, *E. coli* BL21 (negative control); 1, 2, *E. coli* BL21-Mgfp. A. Expression with coomassie-blue-stained SDS-PAGE of whole-cell; B, purification with coomassie-blue-stained SDS-PAGE analysis; C, western blot analysis; D, immobilized metal affinity purification fractions. Lanes: M, protein molecular mass marker; CK, whole-cell of IPTG non-induced (negative control); I, whole-cell of IPTG induced; 1, 2, 4 and 5, purification under denaturing (contained 8 mol/L urea); 3 and 6, purification under natural.

Western blot analyses confirmed that the purified protein was indeed a recombinant Mgfp-5 (Figure 1D).

DOPA content and function analysis

In order to assess the association between DOPA content and protein adhesion, DOPA content was measured. We performed a comparative study with BSA as a negative control and Cell-Tak^{TM} as a positive control. Cell-Tak^{TM} is a commercially available naturally extracted *Mytilus edulis* adhesive-protein mixture of fp-1 and fp-2 that contains DOPA residues in 5% acetic acid buffer. Recombinant Mgfp-5 and Cell-Tak^{TM} was modified, and DOPA content of the modified recombinant Mgfp-5 (9.6 pmol/g) was discovered to be 9.32, 2.35 and 1.58 times higher than that of the unmodified recombinant Mgfp-5 (1.03 pmol/g), unmodified Cell-Tak^{TM} (4.09 pmol/g), and modified Cell-Tak^{TM} (6.07 pmol/g), respectively (Figure 2A). These findings suggested that part of tyrosine residues in recombinant Mgfp-5 had been oxidized to DOPA.

A simple coating assay was performed to test the adhesive ability of recombinant Mgfp-5. As shown in Figure 2B, recombinant Mgfp-5 and Cell-Tak^{TM} could still adhere to the glass surface, while BSA was almost cleared and cleaned after each surface was washed thoroughly with Milli-Q water. The lighter spot color produced indicated that the adhesive intensity of modified recombinant Mgfp-5 was twice as strong as that of unmodified recombinant Mgfp-5, quantified by PDQest software (Figure 2C). This result demonstrated that modified recombinant Mgfp-5 contributed to the improvement of adhesive ability of the recombinant Mgfp-5.

AFM was selected to further investigate the adhesive ability of the recombinant Mgfp-5. As was shown in Figure 2D, adhesive force of modified recombinant Mgfp-5 (~1116.67 nN) was much higher than that of unmodified recombinant Mgfp-5 (~19.67 nN) and Cell-Tak^{TM} (698.33 nN). However, it was interesting that adhesive force of modified Cell-Tak^{TM} showed a descending trend, which might be related to the fact that commercial Cell-Tak^{TM} had already contained enough DOPA, while the intermolecular cross-link of DOPA through oxidizing would affect its adhesive ability, leading to reduced adhesive force.

Adhesion used for laboratory plastic consumables, including spearhead and centrifugal tube cover of different sizes or weights was tested (Figure 2E). It was discovered that modified Mgfp-5 and unmodified Cell-TakTM could easily and completely adhere to these items within 10 min. It took 30 min for the modified Cell-TakTM to complete cross-linking for adhesion. More seriously, adhesion of unmodified recombinant Mgfp-5 took about 12 h or even longer to fall off.

Cytotoxicity test

L-929 cells were incubated in a CO_2 incubator at 37°C and monitored after 2 days. As shown in Figure 3, L-929 cells of blank control group (a) attached well on the bottom of the plate. The online cells were clear with diamond or flattened spindle shape. Cells in negative control (b) and test groups (d) kept normal growth condition with no cytolysis observed, but cell density was slightly lower than that of the blank control group.

The cellular structure in a positive control group (c) was damaged. A large number of black spots were observed in the field of view, indicative of cell death occurring in nearly all cells. CCK-8 assay was used to measure the RGR and cytotoxicity (Table 2). RGR of positive control DMSO was 12.11±0.10% and the cytotoxicity of DMSO was in grade 4. RGR of test group with recombinant Mgfp-5 (RGR_{Mgfp} = 90.36±0.19%) was close to that of positive control (RGR_{PBS} = 93.12±0.07%). The cytotoxicity of recombinant Mgfp-5 was in grade 1 according to Table 1, which means that recombinant Mgfp-5 (9.6 mg/L) has a very good cytocompatibility.

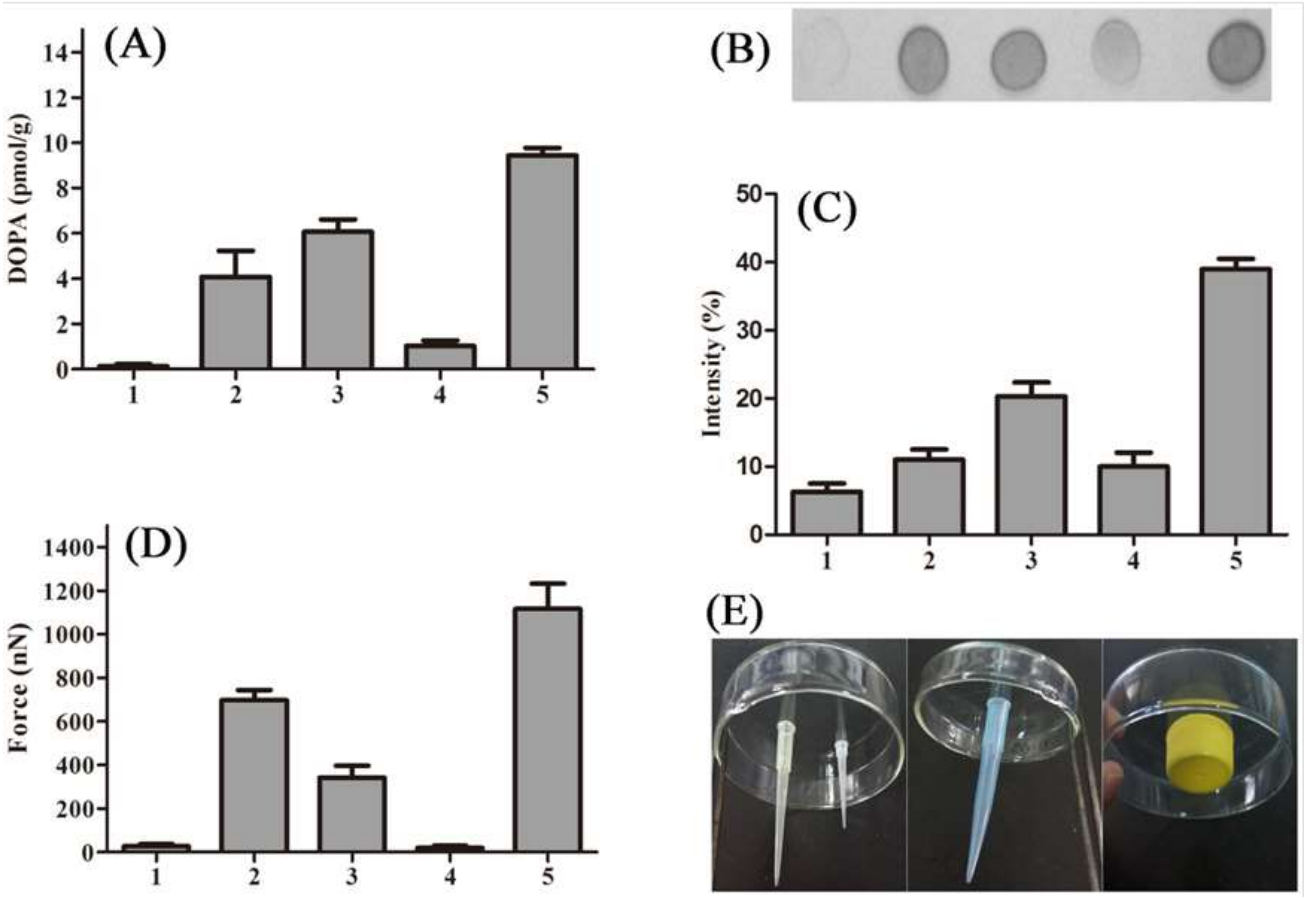

Figure 2. Adhesion ability of the recombinant Mgfp-5, Cell-Tak™ (with or without tyrosinase modification) and BSA. BSA was used as a negative control. (A) DOPA quantity assay; (B) Coating ability assay: 10 µL of 1.00 mg/mL sample was added into the glass surface and incubated under a humid environment at 25°C for 12 h; (C) PDQuest analysis of protein spots on glass: Images of protein spots were captured by a scanner and were analyzed by PDQuest software using uncoated region as control; (D) measurement of adhesion forces of the recombinant Mgfp-5 using modified AFM analysis; (E) macroscopic adhesion phenomenon: adhesion of laboratory plastic consumables using modified Mgfp-5. Each value and error bar represents the mean of triplicate samples and its standard deviation.1-5 represent BSA, unmodified recombinant Cell-Tak™, modified recombinant Cell-Tak™, unmodified recombinant Mgfp-5, modified recombinant Mgfp-5, respectively.

Hemolysis test

Figure 4 displayed the experimental image of hemolysis test with different concentrations and incubation times which was accompanied by a clear sediment and colorless transparent supernatant in groups 1, 2, 3 and negative controls (Sterile 0.9% sodium chloride solution) with hemolysis-free, while positive controls and groups 4 showed a little sediment and bright red supernatant with apparent hemolysis (Table 3).

Table 4 shows that the maximum concentration of Mgfp-5 at 20 µg/mL did not lead to a severe hemolysis within 3 h incubation by hemolysis ratio. Hemolysis ratio of recombinant Mgfp-5 with 20 µg/mL for 3 h was 2.74% (Table 4). According to ANSI/AAMI/ISO 10993-4:2002/A1:2006, the upper limited value of hemolysis index was 5%. Thus, the recombinant Mgfp-5 with 20 µg/mL has no hemolysis.

DISCUSSION

An impediment to further understand the unique adhesion and mechanism of MAPs is the lack of sufficient and pure protein. Large quantities of MAPs are needed to perform research and development for commercial adhesives. Existing approaches for natural extraction of Mgfp-5 are associated with several disadvantages, including low yield, being easily solidified and difficult to purify (Strausberg and Link, 1990), which might have prompted researchers to turn to genetic engineering for protein Mgfp-5 extraction.

Prokaryotic genetic engineering was one of the preferred techniques for example recombinant Mgfp-5 from *M. galloprovincialis* as reported by Hwang et al. (), which was expressed in *E. coli* and only micro test of related function was conducted subsequently, rather than its biosafety (Hwang et al., 2004). Recombinant Mgfp-5

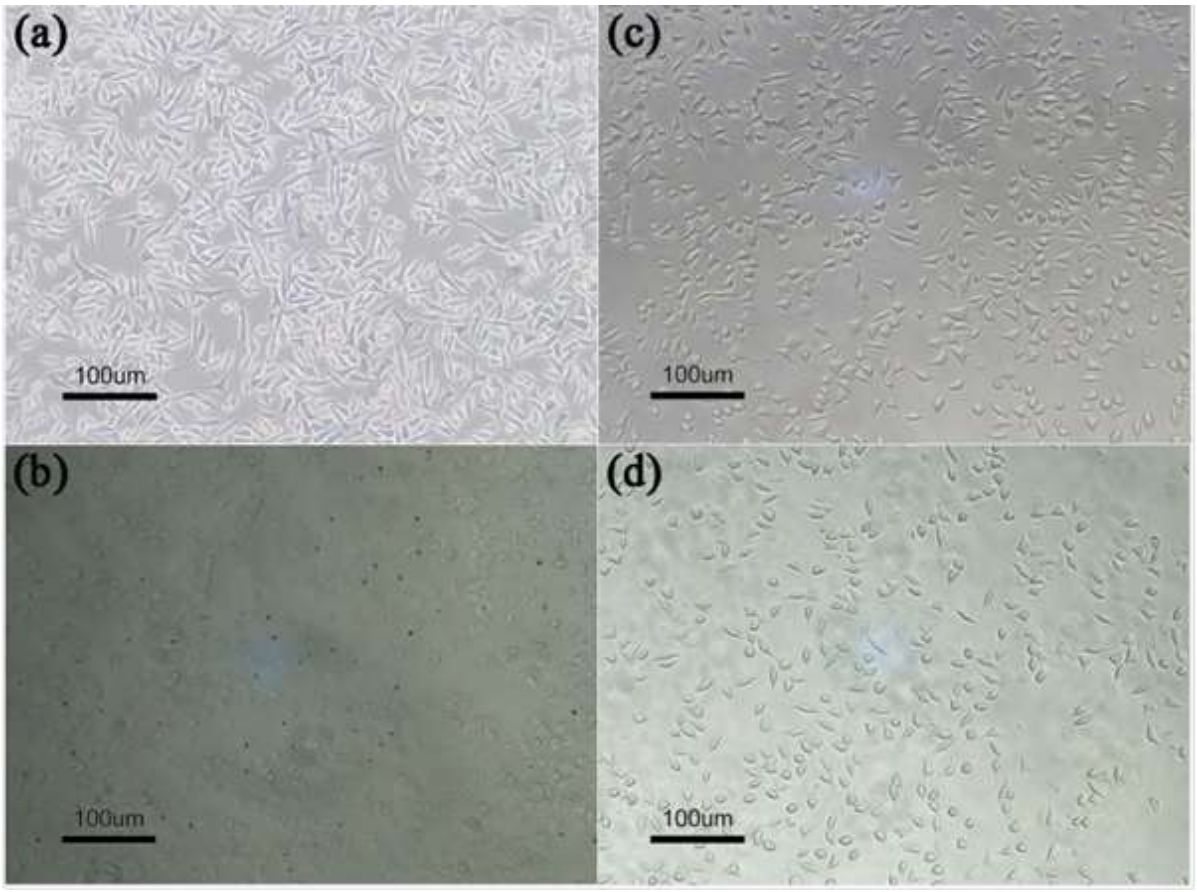

Figure 3. L-929 cells morphology in different culture condition. 100 µL protein solution was added in every well on the base of the concentration of 9.6 mg/L. (a) Cell culture medium DEME; (b) PBS buffer; (c) DMSO; (d) recombinant Mgfp-5.

Table 2. L-929 cells toxicity in different culture condition.

Group	RGR (%)	Cytotoxicity grade
a	100.0±0.00	0
b	93.12±0.07	1
c	12.11±0.10	4
d	90.36±0.19	1

10 µL CCK-8 was added into each well and the absorbance value at 450 nm after 4 h was recorded. Data represent the mean values ± SE (n = 3). (a) Cell culture medium DEME; b, PBS buffer; c, DMSO; d, recombinant Mgfp-5.

was also expressed in *E. coli* after optimizing the conditions for both expression and purification as shown in previous research. This result showed 16% yield and a better purity of 96% (Lv et al., 2016). Under such conditions, the bioreactor was used to produce recombinant Mgfp-5 in quantities (302.00±16.55). The yield of the recombinant Mgfp-5 was increased from 8.3 to 12.25% when 8 mol /L urea was added into the lysis buffer.

Mussel foot has a good adhesion in the water environment. The reason is that the DOPA in the protein has an extremely important role, which is the binding of DOPA to the substrates and the internal cross-linking of the proteins. All these proteins contain DOPA, formed by post-translational modification of tyrosine and have high isoelectric points (IEP) which differ vastly in sequences. Since DOPA can be oxidized and transformed to quinones and thus catalyze 1,2-benzenediols redox cycling at an alkaline pH, in the presence of potassium glycinate as a reductant, the released superoxide reduces NBT to formazan, therefore, allows a specific staining of DOPA-rich proteins (Paz et al., 1988). Then, modified approach of NBT/glycinate staining for the quantitative analysis of DOPA in recombinant Mgfp-5 is used.

Among the MAPs, the protein Mfp-5 had a small molecular-weight which contained a lot of DOPA (about 30%) (Hwang et al., 2004). Recombinant Mgfp-5 in *E. coli* also contained the majority of tyrosine residues, which could be modified to DOPA using tyrosinase (Hwang et al., 2010). However, excessive oxidation of DOPA is

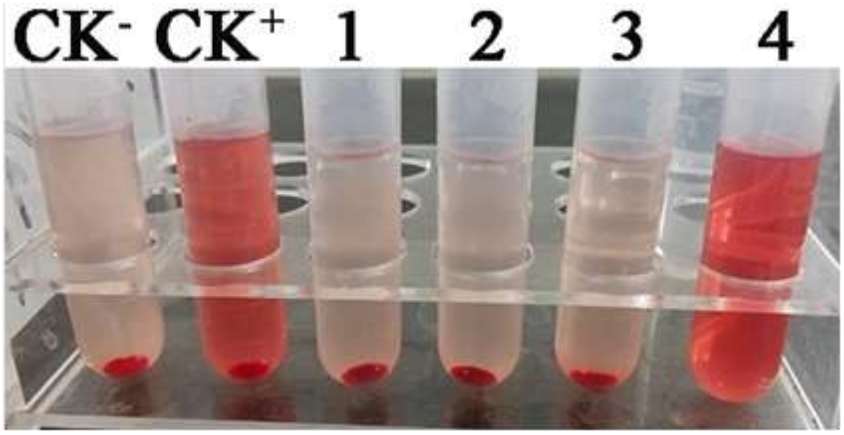

Figure 4. The experimental image of hemolysis test and different concentrations of recombinant Mgfp-5. Lanes, CK^-, Sterile 0.9% sodium chloride solution; CK^+, distilled water; 1-4, represent recombinant Mgfp-5 solution of 5, 10, 20 and 25 µg/mL, respectively.

Table 3. Hemolysis of recombinant Mgfp-5 with different concentrations and incubation times.

Time (h) groups	CK^-	CK^+	1	2	3	4
0.5	-	+	-	-	-	±
1	-	+	-	-	-	+
2	-	+	-	-	-	+
3	-	+	-	-	-	+

"+", completely hemolysis; "-", hemolysis-free "±"; part of the hemolysis, 1-4, represent recombinant Mgfp-5 solution of 5, 10, 20 and 25 µg/mL, respectively.

Table 4. Hemolysis ratio of Mgfp-5 solution with different concentrations for 3 h incubation.

Groups	CK^-	CK^+	1	2	3	4
A	0.058	0.901	0.066	0.071	0.082	0.121
Haemolysis ratio (%)	-	-	0.91	1.49	2.74	7.20

CK^-, Sterile 0.9% sodium chloride solution; CK^+, sterile water; 1-4 represent recombinant Mgfp-5 solution of 5, 10, 20 and 25 µg/mL, respectively.

resulted in self-ligation, rendering reduced protein adhesion. Researchers selected sodium borate and ascorbic acid to maintain the stability and protein adhesion of DOPA (Kan et al., 2014; Tatehata et al., 2000). In this study, sodium borate and ascorbic acid were added to protect DOPA from self-ligation during modification process. It was found in this study that DOPA content of modified recombinant Mgfp-5 (9.6 pmol/g) was about 9.32 times higher than that of unmodified recombinant Mgfp-5 which led to significantly improved adhesion. At the same time, it could also be observed that adhesion of commercial Cell-Tak^{TM} decreased is accompanied by the increase in DOPA content possibly because it typically comes with enough DOPA. DOPA content would be increased while adhesion would be decreased once DOPA was further modified.

Atomic force microscopy was applied in detecting the Surface texture of various materials by atomic-level imaging, through which the surface friction, adhesion force and hardness could be determined. Based on this analysis, the adhesion force of modified recombinant Mgfp-5 was better than that observed in commercialized Cell-Tak^{TM}, which might be due to the combination of Mfp-1 with Mfp-2, as well as the lower content of DOPA than that of Mfp-5 chosen in the commercial Cell-Tak^{TM}. Therefore, both the content of DOPA and the adhesion force of commercialized Cell-Tak^{TM} were inferior to those

of recombinant Mgfp-5 that had been modified by tyrosinase.

Implant materials must have good biocompatibility because they will directly contact with tissues and cells after implanted into body. As a new biomaterial for adhension, it is important to evaluate its biosafety from experimental study to clinical application. The common method is to implant the test material into the body of an animal. However, implantation *in vivo* is limited by the long experimental period, complicated operation process, complex body environment and parameter control, among others (Wang et al., 2012; Lee et al., 2016). In contrast, experiments conducted *in vitro* are relatively simple and their reproducibility can easily be controlled (Li et al., 2015).

In ANSI/AAMI/ISO 10993-5:1999 standards, the cytotoxicity test is generally accepted as the first chosen item on account of convenience, fastness, high sensitivity and saving animal, etc. L929 cells are the first and most widely used cell line in cytotoxic test. L929 cells have the merit of stable passage, fast multiply, low condition for culture *in vitro,* being used for many materials cytotoxic test. The CKK-8 assay is sensitive to detect toxicity of materials and consistent with the toxicity experiment results in animals, which is considered to be a good method in evaluating the cytotoxicity of medical material *in vitro* (Li et al., 2016). According to the rule of MAP wound dressing in the use of the human body (Usage amount of the 2% human body area less than 1 mL per day), the amount of MAP was 3.0 μg/cm^2 (Liu et al., 2013). Therefore, the mass concentration of Mgfp-5 should be 9.6 mg/L on the base of 96 well culture plates.

In the current study, the RGR of recombinant Mgfp-5 at a concentration of 9.6 mg/L is above 90% and cytoxicity is grade 1 at 2 days. Therefore, the recombinant Mgfp-5 is consistent with medical standard of biomaterial. The L-929 cells morphology cultured in recombinant Mgfp-5 had no significant difference as compared to the control and is well attached at the bottom of the culture plate, which demonstrated that recombinant Mgfp-5 had no apparent cytotoxicity and could promote cell proliferation without affecting their normal function.

The hemolysis test is based on the degree of erythrolysis and hemoglobin dissociation while the material contacts RBC *in vitro*. ISO indicate that medical biomaterials which will be applied to the body and to biological tissue ought to be evaluated by the hemolysis test (ANSI/AAMI/ISO 10993-4:2002/A1:2006). Hemolysis is a phenomenon of hemoglobin release which results in erythrolysis. Besides the endogenic hemolytic factors such as abnormity of red blood membranes and hemoglobin, there are some kinds of extrinsic factors such as physic agent on material surface, which can lead to cytotoxicity or may result in machinery damage to RBC. Generally, if hemolysis activity is observed in the hemolysis test, the material shows toxic.

In this study, the fresh rabbit blood was added into the test negative and positive control groups. The results show that the hemolytic ratio of recombinant Mgfp-5 when the concentration was 20 μg/mL is 2.7%, which is lower than the national and international standards of 5%. According to ANSI/AAMI/ISO 10993-4:2002/A1:2006, it suggests that protein with less than 20 μg/mL do not harm the RBC.

CONFLICT OF INTERESTS

The authors have not declared any conflict of interests.

ACKNOWLEDGMENTS

This study was funded by the National natural science foundation of China (31270411; 31572665), the Social Development Science Research plan in Shaanxi province (2012K12-01-02), and the Shaanxi province Department of Education (12JK0827). Yawei Lv designed and performed the entire experiments, Yujing Zhang was responsible for protein purification and data analyses, Wenying Gao performed the adhesion force and toxicity testing and Yingjuan Wang supervised the research. All authors have read and approved the final manuscript.

REFERENCES

ANSI/AAMI/ISO 10993-4:2002/A1:2006 (R2013). Biological evaluation of medical devices - Part 4: Selection of tests for interactions with. blood -Amendment 1. Arlington, VA.

ANSI/AAMI/ISO 10993-5:1999. Biological evaluation of medical devices -Part 5: Tests for cytotoxicity: *In vitro* methods. Arlington, VA.

Dove J, Sheridan P (1986). Adhesive protein from mussels: possibilities for dentistry, medicine, and industry. J. Am. Dent. Assoc. 112(6):879.

Ducker WA, Senden TJ, Pashley RM (1991). Direct measurement of colloidal forces using an atomic force microscope. Nat. 353(6341):239-241.

Gim Y, Hwang DS, Lim S, Song YH, Cha HJ (2008). Production of Fusion Mussel Adhesive fp-353 in Escherichia coli. Biotechnol. Progr. 24(6):1272-1277.

Hwang DS, Yoo HJ, Jun JH, Moon WK, Cha HJ (2004). Expression of Functional Recombinant mussel adhesive protein Mgfp-5 in Escherichia coli. Appl. Environ. Microb. 70(6):3352-3359.

Hwang DS, Zeng H, Masic A, Harrington MJ, Israelachvili JN (2010). Protein-and metal-dependent interactions of a prominent protein in mussel adhesive plaques. J. Biol. Chem. 285(33):25850-25858.

Kan Y, Danner EW, Israelachvili JN, Chen Y, Waite JH (2014). Boronate Complex Formation with Dopa Containing Mussel Adhesive Protein Retards pH-Induced Oxidation and Enables Adhesion to Mica. Plos One 9(10):e108869.

Lee U, Yoo CJ, Kim YJ, Yoo YM (2016). Cytotoxicity of gold nanoparticles in human neural precursor cells and rat cerebral cortex. J. Biosci. Bioeng. 121(3):341-344.

Li L, Gao M, Song B, Zhang H, Wang Y (2016). Effects of RECQ1 helicase silencing on non-small cell lung cancer cells. Biomed. Pharmacother. 83:1227-1232.

Liu Q, Lan H, Gu M, Gao M, Wang Z (2013). Cytotoxicity tests for the mussel adhesive protein dressing for wound healing. Chinese J. Tissue Engineering Research 17(38):6785-6790.

Lv Y, Lv Y, Yang Z, Wang R, Zhang Y, Wang Y (2016). Prokaryotic expression and purification of Mytilus galloprovincialis foot protein-5. J. Northwest. Univ. 46(3):390-396.

Paz MA, Gallop PM, Torrelio, Flückiger R (1988). The amplified detection of free and bound methoxatin (PQQ) with nitroblue tetrazolium redox reactions: insights into the PQQ-locus. Biochem. Biophys. Res. Commun. 154(3):1330-1337.

Platko JD, Deeg M, Thompson V, Al-Hinai Z, Glick H, Pontius K, Colussi P, Taron C, Kaplan DL (2008). Heterologous expression of Mytilus californianus foot protein three (Mcfp-3) in Kluyveromyces lactis. Protein Expres. Purif. 57(1):57-62.

Rego SJ, Vale AC, Luz GM, Mano JF, Alves NM (2016). Langmuir Adhesive Bioactive Coatings Inspired by Sea Life. Langmuir 32(2):560-568.

Silverman H, Roberto F (2007). Understanding marine mussel adhesion. Mar. Biotechnol. 9(6):661-681.

Strausberg RL, Link RP (1990). Protein-based medical adhesives. Trends Biotechnol. 8(2):53-57.

Tatehata H, Mochizuki A, Kawashima T, Yamashita S, Yamamoto H (2000). Model polypeptide of mussel adhesive protein. I. Synthesis and adhesive studies of sequential polypeptides (X-Tyr-Lys)(n) and (Y-Lys)(n). J. Appl. Polym. Sci. 76(6): 929-937.

Waite JH (2002). Adhesion a la moule. Integr. Comp. Biol. 42(6):1172-1180.

Waite JH (2011). Mussel-inspired wet adhesives and coatings. Annu. Rev. Mater. Res. 41:99-132.

Waite JH, Tanzer ML (1981). Polyphenolic substance of *Mytilus edulis*: novel adhesive containing L-Dopa and hydroxyproline. Sci. 212(4498):1038-1040.

Wang F, Wang Z, Tian H, Qi M, Zhai Z, Li S, Lu J (2012). Biodistribution and Safety Assessment of Bladder Cancer Specific Recombinant Oncolytic Adenovirus in Subcutaneous Xenografts Tumor Model in Nude Mice. Curr. Gene. Ther. 12(2):67-76.

Wu C, Han P, Liu X, Xu M, Tian T, Chang J, Xiao Y (2014). Mussel-inspired bioceramics with self-assembled Ca-P/polydopamine composite nanolayer: Preparation, formation mechanism, improved cellular bioactivity and osteogenic differentiation of bone marrow stromal cells. Acta Biomater. 10(1):428-438.

Yu M, Hwang J, Deming TJ (1999). Role of L-3, 4-dihydroxyphenylalanine in mussel adhesive proteins. J. Am. Chem. Soc. 121(24):5825-5826.

African Journal of Biotechnology

Related Journals Published by Academic Journals

- *Biotechnology and Molecular Biology Reviews*
- *African Journal of Microbiology Research*
- *African Journal of Biochemistry Research*
- *African Journal of Environmental Science and Technology*
- *African Journal of Food Science*
- *African Journal of Plant Science*
- *Journal of Bioinformatics and Sequence Analysis*
- *International Journal of Biodiversity and Conservation*

academicJournals